Theoretical and Experimental Study of Noise Behavior of Microwave Active Filters

Hil-Yee Chan, Walter

A Thesis Submitted in Partial Fulfillment

of the Requirements for the degree of

Master Philosophy

In

Electronic Engineering

July, 2000


香港中文大學
大學
圖書館系統
28 JUN 2001
UNIVERSITY
LIBRARY SYSTEM
THE CHINESE UNIVERSITY OF HONG KONG

Abstract

Narrow-band filters are widely used in many microwave systems. MMIC technology offers the attractive advantages of size reduction and higher functional integration than that of traditionally passive filter. Unfortunately, at microwave frequencies, the Q-factor of the on-chip inductors is typically low and, hence, passive narrow-band MMIC filters usually exhibit high insertion loss and poor selectivity.

In recent years, the negative resistance techniques have been proposed for use in MMIC filters to compensate the component losses, especially of the spiral inductors. These techniques enable the design of microwave active filter with zero insertion loss and excellent channel selectivity.

A prime factor in determining the sensitivity of a receiver chain is the noise figure of the components which include RF filters. This thesis presents the detail analysis of noise performance of the microwave band-pass filters based upon the negative-resistance method. Furthermore, circuit techniques to minimize the noise figure of the filter will be addressed.

For demonstration, experimental filter circuits operated at about 900MHz are constructed and tested. It is also found that, with the proper choice of component values, the filter's noise figure can be optimized at the sacrifice of its linearity performance.

摘要

窄頻帶濾波器於微波系統中已被廣泛應用。在微波頻率下，電感器之 Q 值一般是較低的，因此無源窄頻帶濾波器之插入損耗相當高，而選擇性亦較差。最近有多個研究報告發表了利用負電阻之技術，對無源濾波器之元件損耗作補償，使濾波器可達致低插入損耗，並提高選擇性。

在接收器中，各零件之雜訊指數，包括濾波器，均會對整個接收器的靈敏度有重要的影響。在這論文中，將會對利用負阻作保賞之有源濾波器的噪聲問題作詳細分析，並找出降低有源濾波器雜訊指數之方法。同時，九百兆赫有源濾波器的實驗性混合電路亦被製成並測試，以驗證這有關降低雜訊指數之理論。測量結果顯示，在濾波器中選擇適當的零件值，可犧牲其線性表現而獲得較佳之雜訊指數。

Acknowledgement

I would like to express my grateful acknowledgement to my supervisor, Prof. K. K. Cheng, for his guidance and enlightenments throughout the course of research. Also, I would like to express my gratitude to my parents and my family, for their love and support. Special thanks to my girl friend, Annie, for her understanding and care. Last but not least, my sincere thanks to Mr. C. W. Fan, Mr. K. C. Ho, and Mr. P. H. Kwok, my colleague, for their encouragement.

Table of Content

Chapter 1 Introduction

Due to the rapid growth of wireless market, many companies have been working hard on the development of transceiver chipsets. Quite a number of chipsets which combine functions of transmit and receive modules for GSM and DECT applications have been made available in the last couple of years. Unfortunately, filtering functions are still placed off-chip in almost all available chipsets. Commercially available ceramic resonator has Q-factors in the range of 400-600. SAW and ceramic filter seem to be a solution but they have created several problems such as size incompatibilities, parasitic effect and pass-band dissipative losses.

The use of MMIC technology to realize microwave filters would clearly be advantageous for the above problems because of the potential of great reduction in size. However, at microwave frequencies, the Q-factor of the on-chip inductors is typically very low and, hence, passive narrow-band MMIC filters usually exhibit high insertion loss and poor sensitivity.

MMIC active filters is one of the solutions for the above problems as they not even have zero insertion loss but have the potential for producing gain within the pass-band while providing increased selectivity in out-of-band region. Recent research on active filters can be categorized into four different classes. These include:

a class developed from the adaptation of low frequency active filter synthesis techniques to microwave filter design [3-4], another class employing the use of negative resistance to compensate for the losses of resonators [5-11], a class incorporating the transversal and recursive filter approach [12-15], and a final class involving novel types of active resonator, e.g. the active inductor [16-17] and the active feedback resonator [18].

However, for active band-pass filters to become an alternative to their passive counterparts in microwave receivers, two critical problems are needed to be addressed: intermodulation distortion(IMD) and noise performance of the filter circuit. Due to the inherent nonlinearity of active device, undesirable IMD can be produced when two or more signals are applied to the filter simultaneously. Particularly, the third-order IMD has severe effects on the performance of most communication systems. Recently, Cheng and Chan reported a detail analysis of the IMD of an active band-pass filters based upon Volterra series formulation [9].

On the other hand, the noise figures of the active filters should be comparable to those of the passive filters. Unfortunately, only a few authors have investigated the noise performance of their proposed active filter [2, 4, 7, 11, 14, 15,18]. Most of them have just measured the noise performance of their active filter. [2] presented a computer oriented technique to predict and quantify the noise figure of various active

filter types while [15, 18] proposed two analytical approaches for noise figure evaluation for a certain types of active filter circuit.

The aim of this project is to examine, both theoretically and experimentally, how the noise figure of an active band-pass filter using MESFET devices may be optimized. This thesis is divided into eight chapters. Chapter 2 is the background theories on coupled-resonator filter design. Chapter 3 details the linear analysis of the negative resistance compensated band-pass filter. Requirement on circuit parameters for the design of zero insertion loss filter are also addressed. Chapter 4 gives a review on the IM analysis of the active filter. Chapter 5 gives a brief description of the noise theory and a method to extract the noise parameter of the MESFET. Chapter 6 presents the noise analysis of the active filter and a new technique for the optimization of the filter's noise figure. Experimental verification of the proposed theories is given in chapter 7. Finally, chapter 8 concludes this thesis and gives some recommendation for future work.

Chapter 2 Background Theory

In most design of passive filters, the insertion loss method is used. This method uses network synthesis techniques to design filters with a specified frequency response, such as the maximally flat and the equal-ripple filter characteristics. The procedure is carried out with low-pass filter prototypes which are normalized in terms of impedance and frequency. Transformations are then applied to convert the prototype designs to a band-pass characteristic with desired frequency range and impedance level.

2.1 Maximally Flat Filter Response

This characteristic is also called the binomial or Butterworth response, and is optimum in the sense that it provides the flattest possible pass-band response for a given filter complexity, or order. The power loss ratio for a maximally flat low-pass filter is

$$L_{A(dB)} = 10\log\left(1+\delta\left(\frac{\omega}{\omega_c}\right)^{2N}\right) \tag{2.1}$$

where

ω_c = cutoff frequency

N = filter order

$$\delta = 10^{\frac{L_{Ar}}{10}} - 1$$

L_{Ar} = attenuation at ω_c

The element values of the filter is

$$g_n = 2\sin\left[\frac{(2n-1)\pi}{2N}\right] \tag{2.2}$$

where

$$n = 1, 2, \ldots, N$$

The values of g_n for $N = 1$ to 5 are listed in table 2.1.

N	g_1	g_2	g_3	g_4	g_5	g_6
1	2	2				
2	1.4142	1.4142	1			
3	1	2	1	1		
4	0.7654	1.848	1.848	0.7654	1	
5	0.618	1.618	2	1.618	0.618	1

Table 2.1 Values of g_n for $N = 1$ to 5

Fig. 2.1 shows the circuit configuration of the maximally flat low-pass filter with order N. The values of the inductance and capacitance are given by

$$C_n = \frac{g_n}{\omega_c Z_o} \tag{2.3}$$

$$L_n = \frac{g_n Z_o}{\omega_c} \tag{2.4}$$

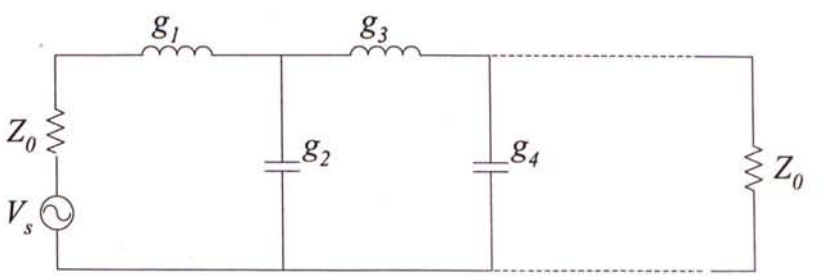

Fig. 2.1. Topology of maximally flat low-pass filter

2.2 Equal-Ripple Filter Response

This characteristic is also called the Chebyshev filter because a Chebyshev polynomial is used to specify the insertion loss of an N^{th}-order low-pass filter. The Chebyshev response would satisfy a requirement for a shaper cutoff than that of Butterworth response. The power loss ratio for the Chebyshev filter is

$$L_{A(dB)} = 10\log\left[1 + k^2 C_N^2(x)\right] \tag{2.5}$$

$C_N(x)$ = Chebyshev polynomial to the order N evaluated at x.

$$k = \sqrt{10^{\frac{r}{10}} - 1}$$

r = pass-band ripple

N = filter order

The Chebyshev polynomials for the first three orders are given in the following equations:

$$C_1 = x \tag{2.6}$$

$$C_2 = 2x^2 - 1 \tag{2.7}$$

$$C_3 = 4x^3 - 3x \tag{2.8}$$

The design equations of Chebyshev filter with r dB pass-band ripple are

$$g_1 = \frac{2\sin\left(\frac{\pi}{2N}\right)}{\sinh\left(\frac{\beta}{2N}\right)} \tag{2.9}$$

$$g_n = \frac{4\sin\left(\frac{2n-3}{2N}\pi\right)\sin\left(\frac{2n-1}{2N}\pi\right)}{b_{n-1}g_{n-1}} \tag{2.10}$$

where

$$n = 1, 2, \ldots, N$$

$$g_{N+1} = \begin{cases} 1 & \text{for N is odd} \\ 2k^2 + 1 - 2k\sqrt{1+k^2} & \text{for N is even} \end{cases} \tag{2.11}$$

$$b_n = \sinh\frac{\beta}{2N} + \sin^2\left(\frac{n\pi}{N}\right)$$

$$\beta = \ln\left(\frac{\sqrt{1+k^2}+1}{\sqrt{1+k^2}-1}\right)$$

The topology of the equal-ripple filter is the same as that of the maximally flat filter in Fig. 2.1, except the terminating resistance may not be the same and the ratio is dependent on the filter order.

2.3 Low-pass to Band-pass Transformation

Band-pass filters can be easily designed with the use of its low-pass filter counterparts. When the low-pass filter is transformed to the band-pass filter, the alternating inductance and capacitance in the low-pass filter are replaced by alternating series and shunt resonator as shown in Fig. 2.2.

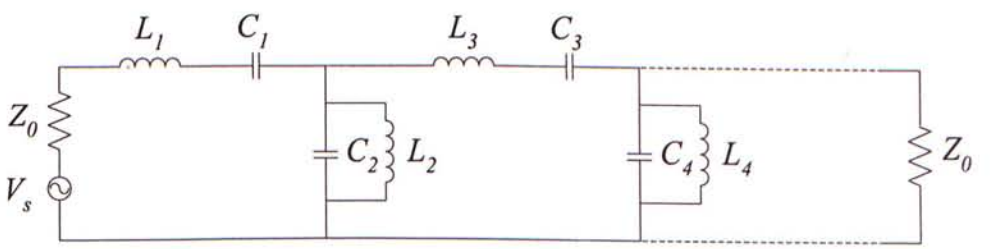

Fig. 2.2 Topology of band-pass filter

The transforming equations for shunt elements g_n are

$$C_n = \frac{g_n}{2\pi Z_0 B} \tag{2.11}$$

$$L_n = \frac{Z_0 B}{2\pi f_0^2 g_n} \tag{2.12}$$

and the transforming equations for series elements g_n are

$$C_n = \frac{B}{2\pi f_0^2 g_n Z_0} \tag{2.13}$$

$$L_n = \frac{Z_0 g_n}{2\pi B} \tag{2.14}$$

where

B = 3dB bandwidth of the filter

f_0 = the center frequency of the filter

2.4 Impedance and Admittance Inverter

An idealized impedance inverter, shown in Fig. 2.3, operates like a quarter-wavelength line of characteristic impedance K and at all frequencies. Therefore, if it is terminated by an impedance Z_b at one end, the impedance Z_a seen looking in at the other end is

$$Z_a = \frac{K^2}{Z_b} \tag{2.15}$$

Fig. 2.4 shows four basic circuits of impedance inverter. Fig. 2.4(a) and Fig. 2.4(b) are particularly useful in circuits where the negative L or C can absorbed into adjacent positive series elements of the same type so as to give a resulting circuits having all positive elements. The inverter parameters K are the image impedance of

the inverter networks.

Similarly, an idealized admittance inverter, shown in Fig. 2.5, operates like a quarter-wavelength line of characteristic admittance J at all frequencies. If an admittance Y_b is terminated at one end, the admittance Y_a seen looking in the other end is

$$Y_a = \frac{J^2}{Y_b} \tag{2.16}$$

Fig. 2.6 shows four basic circuits of admittance inverter, These circuits will be seen to be the duals of those in Fig. 2.4, and the inverter parameters J are the image admittance of the inverter networks.

An inverter may have an image phase shift of either ± 90 degrees or an odd multiple of it. Because of the inverting action, a series inductance with an inverter on each side looks like a shunt capacitance from its exterior terminals. Likewise, a shunt capacitance with an inverter in both sides looks like a series inductance from its external terminals.

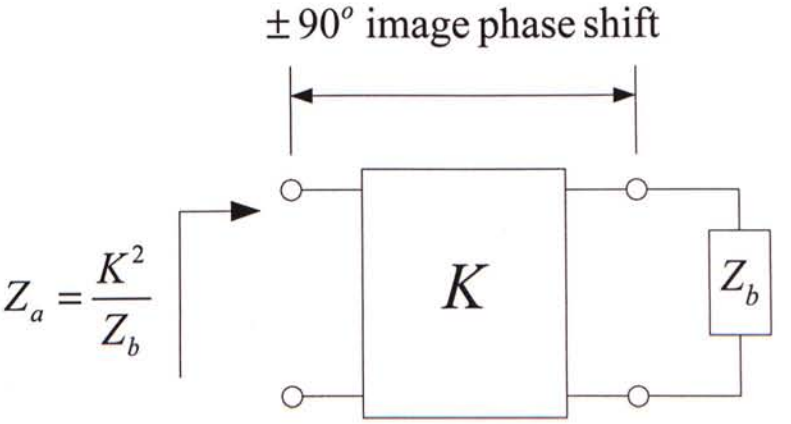

Fig. 2.3 Impedance inverter

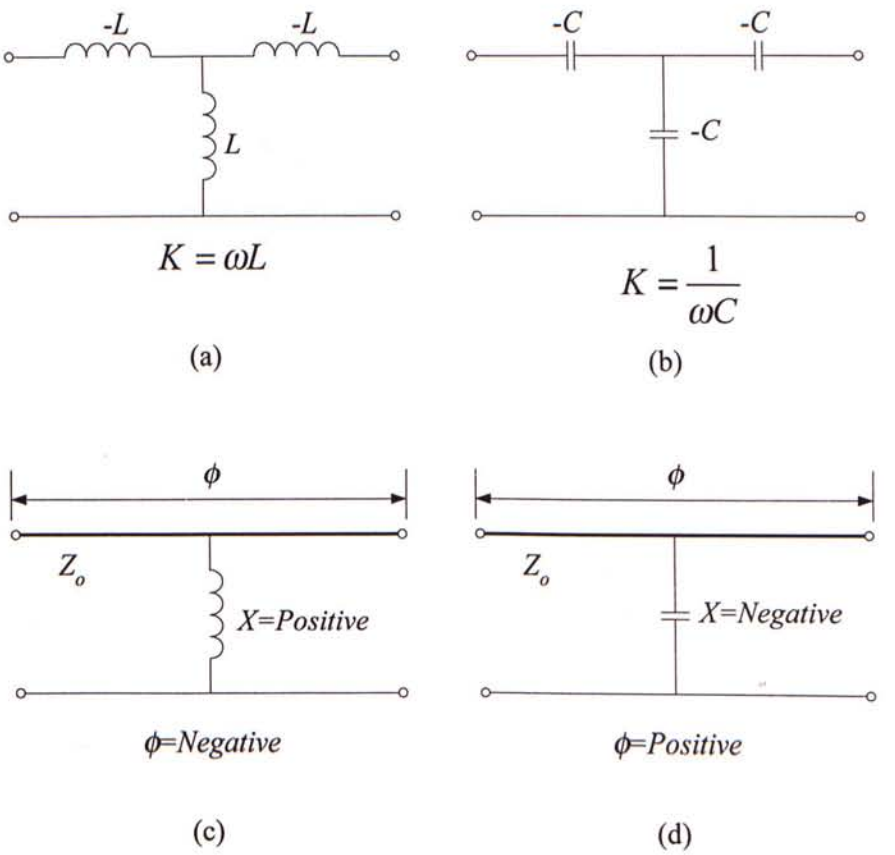

Fig. 2.4 Circuits which are useful as K-inverters

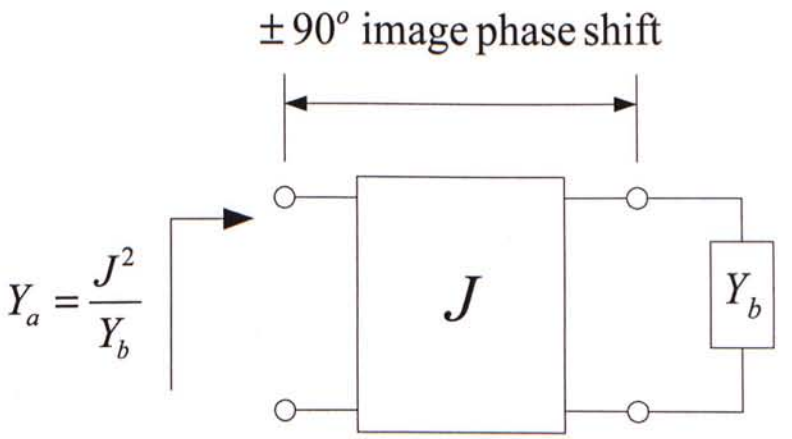

Fig. 2.5 Admittance inverter

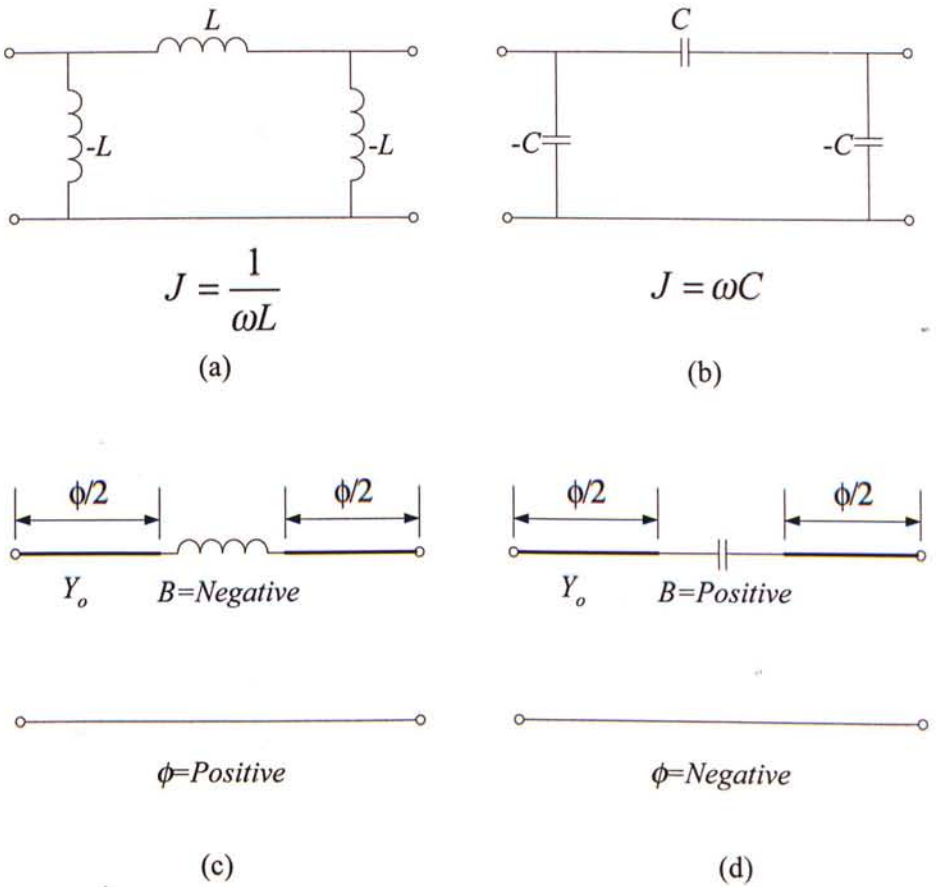

Fig. 2.6 Circuits which are useful as J-inverter

2.5 Coupled-Resonator Filter

By using admittance inverters, the band-pass filter can be converted into a network using only parallel tuned circuits. Furthermore, by choosing the inverter correctly, all of the inductors and capacitors can be chosen to have the same values. With the help of Fig. 2.7 [1], the general expressions for the resonator and $J_{k,k-1}$ for a filter with N resonator are

$$L_{rk} = \frac{1}{C_{rk}\omega_0^2} \qquad \text{k} = 1, 2, \ldots \text{N} \tag{2.17}$$

$$J_{01} = \sqrt{\frac{G_A \omega_0 C_{r1} \Delta}{g_o g_1}} \tag{2.18}$$

$$J_{k,k+1} = \Delta\omega_0 \sqrt{\frac{C_{rk} C_{rk+1}}{g_k g_{k+1}}} \tag{2.19}$$

$$J_{N,N+1} = \sqrt{\frac{G_B \omega_0 C_{rN} \Delta}{g_N g_{N+1}}} \tag{2.20}$$

where

ω_U is the upper cutoff frequency

ω_L is the lower cutoff frequency

$$\Delta = \frac{\omega_U - \omega_L}{\omega_0}$$

$$\omega_0 = \sqrt{\omega_U \omega_L}$$

The capacitances of the inverters are:

$$C_{01} = \frac{J_{01}}{\omega_0 \sqrt{1-\left(\frac{J_{01}}{G_A}\right)^2}} \tag{2.21}$$

$$C_{k,k+1}\Big|_{k=1 \text{ to } N-1} = \frac{J_{k,k+1}}{\omega_0} \tag{2.22}$$

$$C_{N,N+1} = \frac{J_{N,N+1}}{\omega_0 \sqrt{1-\left(\frac{J_{N,N+1}}{G_B}\right)^2}} \tag{2.23}$$

$$C_{01}^{e} = -\frac{C_{01}}{1+\left(\frac{\omega_0 C_{01}}{G_A}\right)^2} \tag{2.24}$$

$$C_{N,N+1}^{e} = -\frac{C_{N,N+1}}{1+\left(\frac{\omega_0 C_{N,N+1}}{G_B}\right)^2} \tag{2.25}$$

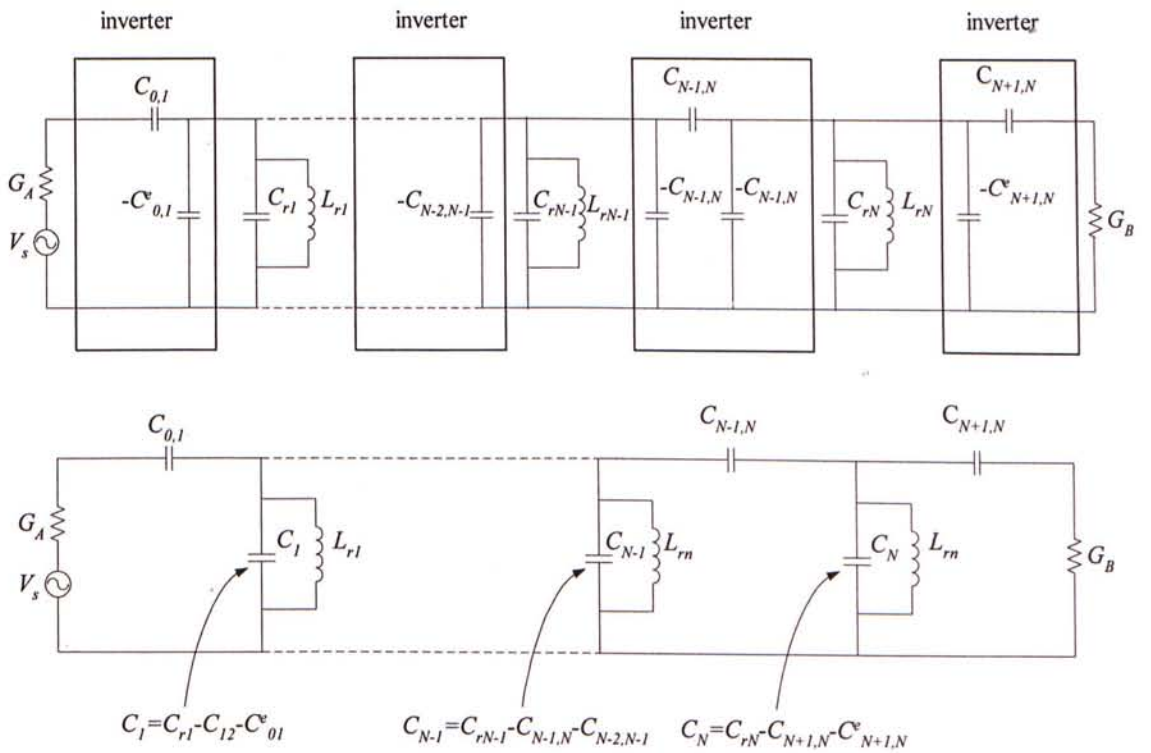

Fig. 2.7 Topology of coupled-resonator filter

Fig. 2.8, Fig. 2.9 and Fig. 2.10 shows the circuits of the second, third and forth order coupled-resonator filter respectively. The expressions of their circuit elements are given as follow.

For the second order coupled-resonator filter,

$$\omega_0 C_r = \frac{1}{\omega_0 L_r} \tag{2.26}$$

$$\omega_0 C_{12} = \frac{1}{1.414\omega_0 L_r}\left(\frac{\omega_U - \omega_L}{\omega_0}\right) \tag{2.27}$$

$$\omega_0 C_{01} Z_0 = \sqrt{\frac{\omega_0 C_{12} Z_0}{1-\omega_0 C_{12} Z_0}} \tag{2.28}$$

$$C_{r1} = C_r - C_{12}\frac{C_{01}}{1+(\omega_0 C_a Z_0)^2} \tag{2.29}$$

For third order coupled-resonator filter,

$$\omega_0 C_{12} = \left(\frac{\omega_U - \omega_L}{\omega_0}\right)\frac{1}{\sqrt{2}\omega_0 L_r} \tag{2.30}$$

$$\omega_0 C_{01} Z_0 = \sqrt{\frac{\sqrt{2}\omega_0 C_{12} Z_0}{1-\sqrt{2}\omega_0 C_{12} Z_0}} \tag{2.31}$$

$$C_{r1} = C_r - C_{12} - \frac{C_{01}}{1+(\omega_0 C_{01} Z_0)^2} \tag{2.32}$$

$$C_{r2} = C_r - 2C_{12} \tag{2.33}$$

For forth order coupled-resonator filter,

$$\omega_0 C_{12} = \left(\frac{\omega_U - \omega_L}{\omega_{0o}}\right)\frac{1}{\omega_0 L_r \sqrt{0.7654\times 1.848}} \tag{2.34}$$

$$\omega_0 C_{23} = \left(\frac{\omega_U - \omega_L}{\omega_0}\right)\frac{1}{\omega_0 L_r 1.848} \tag{2.35}$$

$$\omega_0 C_{01} Z_0 = \sqrt{\frac{\omega_0 \frac{C_{12}^2}{C_{23}} Z_0}{1-\omega_0 \frac{C_{12}^2}{C_{23}} Z_0}} \tag{2.36}$$

$$C_{r1} = C_r - C_{12} - \frac{C_{01}}{1+(\omega_0 C_{01} Z_0)^2} \tag{2.37}$$

$$C_{r2} = C_r - C_{12} - C_{23} \tag{2.38}$$

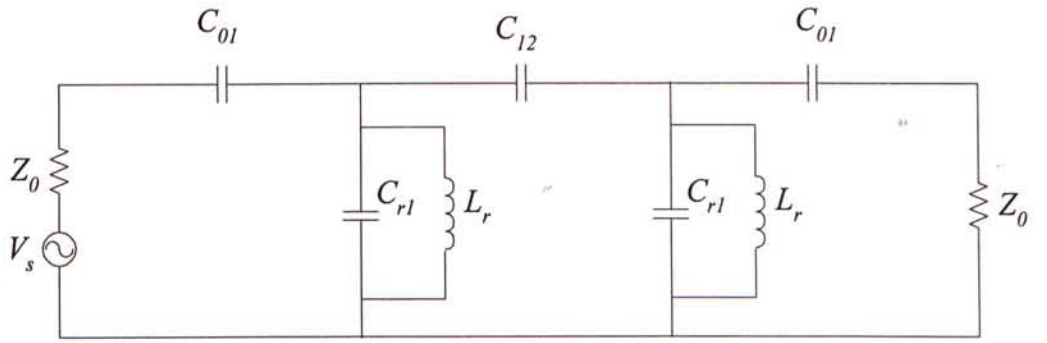

Fig. 2.8 Second order coupled-resonator filter

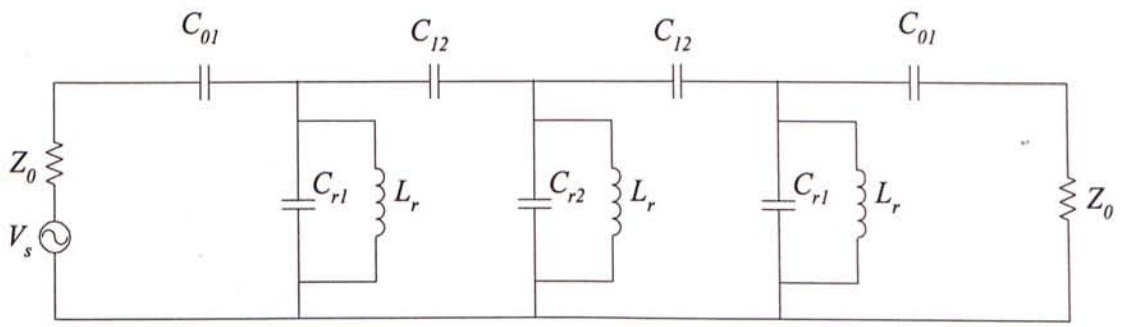

Fig. 2.9 Third order coupled-resonator filter

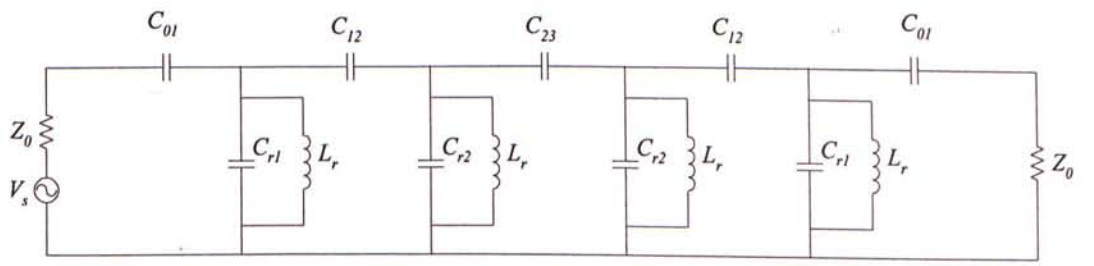

Fig. 2.10 Forth order coupled-resonator filter

Chapter 3 Active Filter Employing Negative Resistance

Direct coupling of negative resistance circuits to coupled-resonator filter has been widely used due to its simplicity in structure. This chapter focuses on the design of the negative resistance circuits using MESFETs, and the derivation of the circuit parameters of the active filter.

3.1 Lossy Coupled-Resonator Filter

The coupled-resonator filter mentioned in chapter 2 is constructed by lossless lumped elements. However, in reality, parasitic elements like stray capacitance, lead or trace inductance and resistance exists in the lumped elements. Frequency shift and insertion loss will be encountered due to these parasitics. The dominant effect is contributed by the lossy inductor which may be considered as a series combination of a lossless inductor and a resistor. Fig. 3.1 shows the circuit of a second-order coupled-resonator filter with the presence of lossy inductors.

The frequency response of a typical second-order coupled-resonator filter, operating at 900MHz has been simulated by MDS^{TM}. The effect of R_r (0Ω, 0.5Ω and 1Ω) upon the filter response is also shown in Fig. 3.2 for comparison. The diagram

indicated that the filter response degrades quite significantly, even for a small value of R_r.

Moreover, the impedance of the lossy inductor can be described as

$$Z_L = R_r + j\omega L_r \tag{3.1}$$

or

$$\begin{aligned} Y_L &= \frac{1}{R_r + j\omega L_r} \\ &= g_o + \frac{1}{j\omega L_r'} \end{aligned} \tag{3.2}$$

where

$$g_o = \frac{1}{R_r\left(1+Q_L^2\right)} \approx \frac{1}{R_r Q_L^2}$$

$$L_r' = L_r\left(1+Q_L^{-2}\right) \approx L_r$$

$$Q_L = \frac{\omega L_r}{R_r}$$

As a result, the resonator in Fig. 3.1 can be transformed into a parallel *RLC* circuit as depicted in Fig. 3.3, under narrow-band assumption.

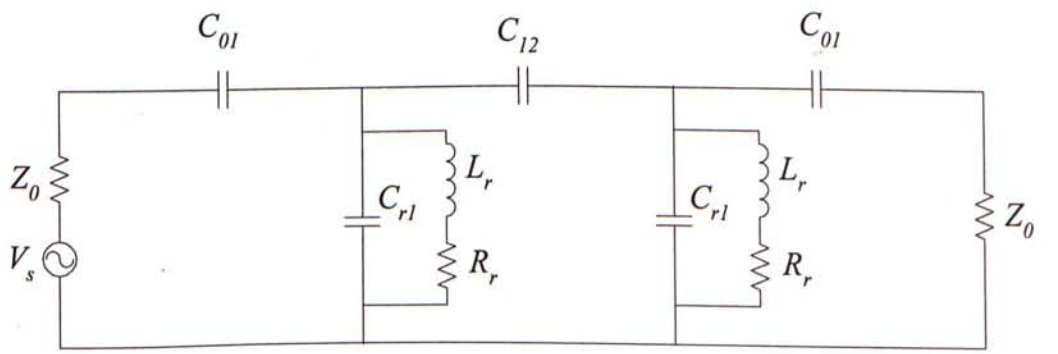

Fig. 3.1 Second Order Coupled-Resonator Filter

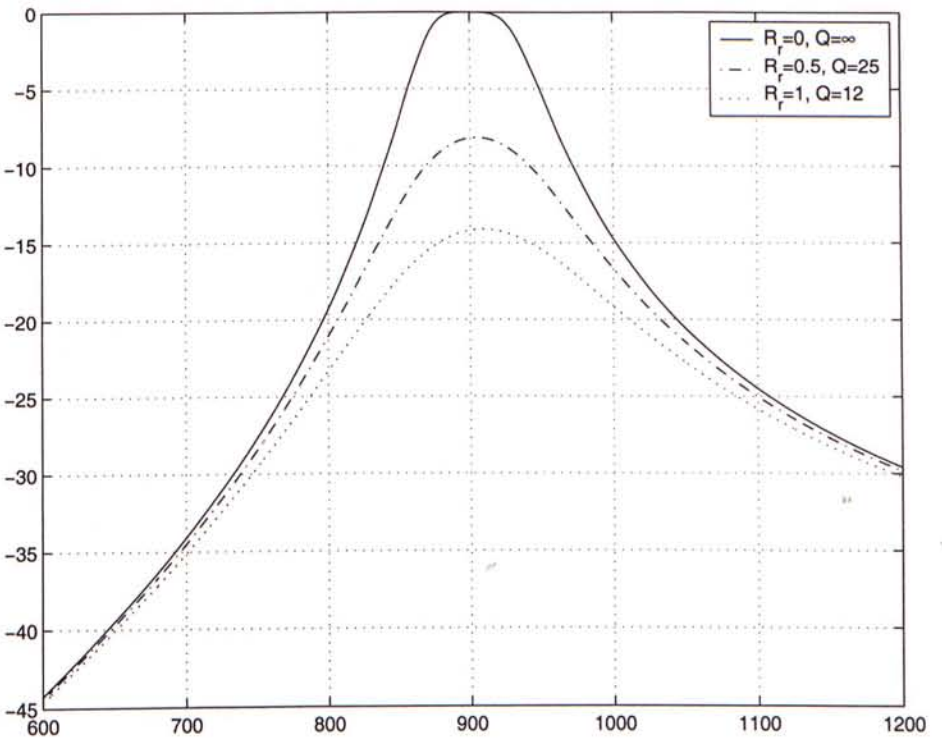

Fig. 3.2 Comparison of S_{21} of ideal and lossy coupled-resonator passive filter

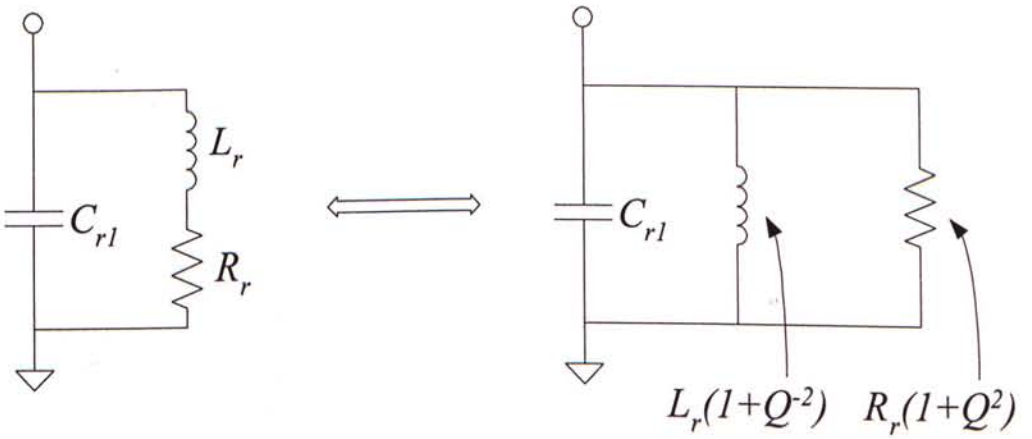

Fig. 3.3 Lossy *LC*-resonator equivalent circuit

3.2 Common-source Capacitive Feedback Circuit

The common-source capacitive feedback topology is employed here as the negative-resistance network for compensating the loss of the resonator. Fig. 3.4 shows the negative resistance circuit which basically comprises a MESFET, a feedback capacitor C_f, and an external gate-to-source capacitor C_{ext}. In the figure, $Z_s(\omega)$ represents the circuit impedance of the bias network, which behaves as an open circuit at high frequencies. For simplicity, only the dominant elements of a MESFET's equivalent model is considered.

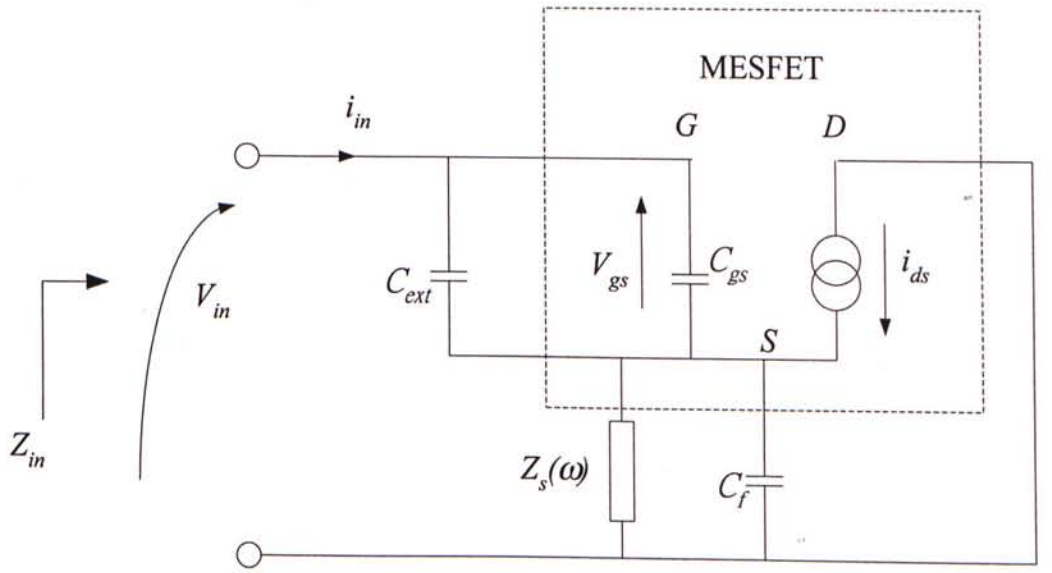

Fig. 3.4 Negative Resistance Circuit

Referring to Fig. 3.4, the input impedance of the negative resistance circuit is [5]

$$\begin{aligned} Z_{in} &= \frac{v_{in}}{i_{in}} \\ &= \frac{-g_m}{\omega^2 C_f C_{gs}} + \frac{1}{j\omega C_T} + \frac{1}{j\omega C_f} \\ &= R_n + \frac{1}{j\omega C_p} \end{aligned} \tag{3.3}$$

where

$$R_n = \frac{-g_m}{\omega^2 C_f C_T}$$

$$C_p = \frac{C_T C_f}{C_T + C_f}$$

$$C_T = C_{ext} + C_{gs}$$

This impedance, Z_{in}, is therefore equivalent to a series combination of a capacitor, C_p, and a negative resistance R_n. For further analysis, the negative resistance circuit is converted into a shunt combination of a resistance, R_{neg} and a capacitance, C_{neg} as shown in Fig. 3.5, where

$$R_{neg} = R_n\left(1 + \frac{1}{\omega^2 C_p^2 R_n^2}\right) \tag{3.4}$$

$$C_{neg} = \frac{C_p}{\left[1 + \left(\omega C_p R_n\right)^2\right]} \tag{3.5}$$

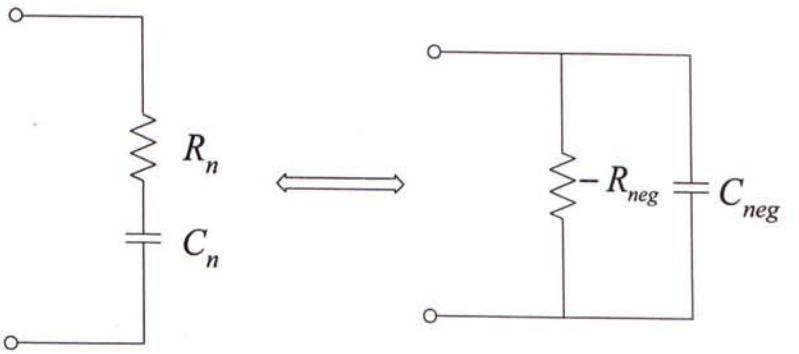

Fig. 3.5 Equivalent circuit of negative resistance

Thus , (3.4) and (3.5) can be rewritten as [9]

$$R_{neg} = \frac{\left(\frac{\alpha}{\beta}\right)^2 + \left(1+\frac{C_f}{C_T}\right)^2}{g_o \alpha \frac{C_f}{C_T}} \tag{3.6}$$

$$C_{neg} = \left(1+\frac{C_f}{C_T}\right)\frac{C_T}{\alpha R_{neg} g_o} \tag{3.7}$$

where

$$\alpha = \frac{g_m}{g_o}$$

$$\beta = \frac{\omega_o C_T}{g_o}$$

3.3 Active *LC*-resonator

An active *LC*-resonator is formed by coupling the negative resistance circuit to the resonator as illustrated in Fig. 3.7. With the help of Fig. 3.3 and Fig. 3.5, the active *LC*-resonator can be represented by the passive shunt *LRC* resonator in parallel with a negative resistance network as depicted in Fig. 3.8. The condition for complete cancellation of the inductor loss by the negative resistance circuit is

$$R_{neg} g_o = 1 \tag{3.8}$$

The addition of the negative resistance circuit will change the resonant frequency of the resonator due to excess shunt capacitance C_{neg}. Because of this, the original capacitance in the resonator has to be adjusted to absorb the extra capacitance to

maintain the original resonant frequency. The overall active *LC*-resonator may now be considered as a lossless resonator.

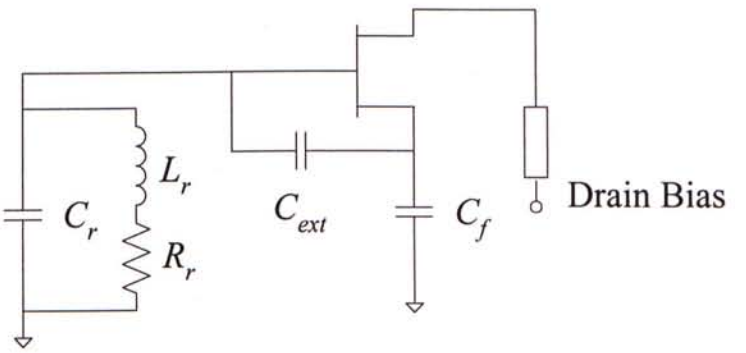

Fig. 3.7 Active *LC*-resonator

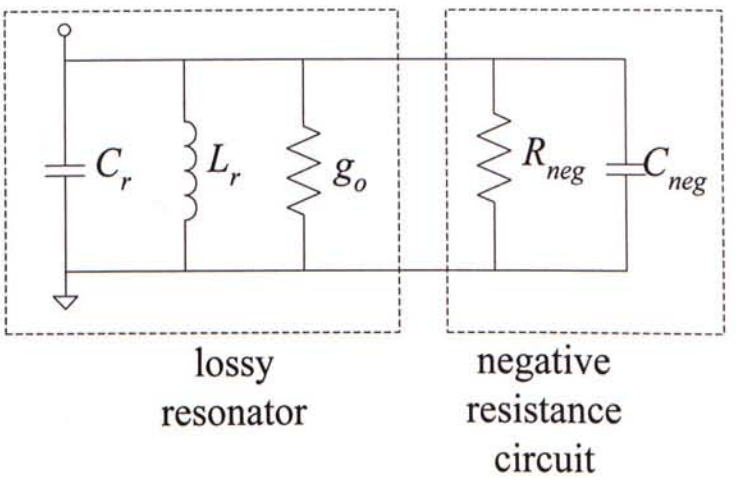

Fig. 3.8 Equivalent circuit of active *LC*-resonator

3.4 Design Criteria of the Active Filter

In designing coupled-resonator active filter, the circuit can be considered as two parts: the passive filter structure and the negative resistance circuit. The passive filter structure can be constructed based upon the procedure described in chapter 2. Equation (3.3) shows that the following parameters are crucial for the exact cancellation of the inductor loss.

1. transconductance g_m

2. gate-source capacitance C_{gs} and the external gate-to-source capacitor C_{ext}

3. external feedback capacitance C_f

As mentioned before, the exact cancellation of inductor loss by the negative resistance circuit is $R_{neg}g_o = 1$. This condition can be re-expressed as:

$$\left(1+\frac{C_f}{C_T}\right)^2+\left(\frac{\alpha}{\beta}\right)^2=\alpha\frac{C_f}{C_T} \tag{3.9}$$

$$C_{neg}=\left(1+\frac{C_f}{C_T}\right)\frac{C_T}{\alpha} \tag{3.10}$$

The solutions of (3.9) are

$$\frac{C_f(\pm)}{C_T}=\frac{\alpha}{2}-1\pm\sqrt{\alpha\left(\frac{\alpha}{4}-1\right)-\left(\frac{\alpha}{\beta}\right)^2} \tag{3.11}$$

where $C_{f(+)} > C_{f(-)}$ provided that

$$g_m > 4g_o \tag{3.12}$$

$$C_{gs} > \frac{2g_o}{\omega\sqrt{1-\frac{4}{\alpha}}} \tag{3.13}$$

$$C_{neg} < C_r \tag{3.14}$$

For illustration, the variation of $R_{neg}g_o$ as a function of $\frac{C_f}{C_T}$ and β (for $\alpha = 8$) is plotted in Fig.3.9. It is clearly shown in the figure that there are two distinct values of $\frac{C_f}{C_T}$ which may be used for exact cancellation of the inductor loss. For larger value of β, the difference between $C_{f(+)}$ and $C_{f(-)}$ is increased. Generally speaking, the values

of R_{neg} and C_{neg} are both frequency dependent and thus, this technique is usable only for narrow-band applications.

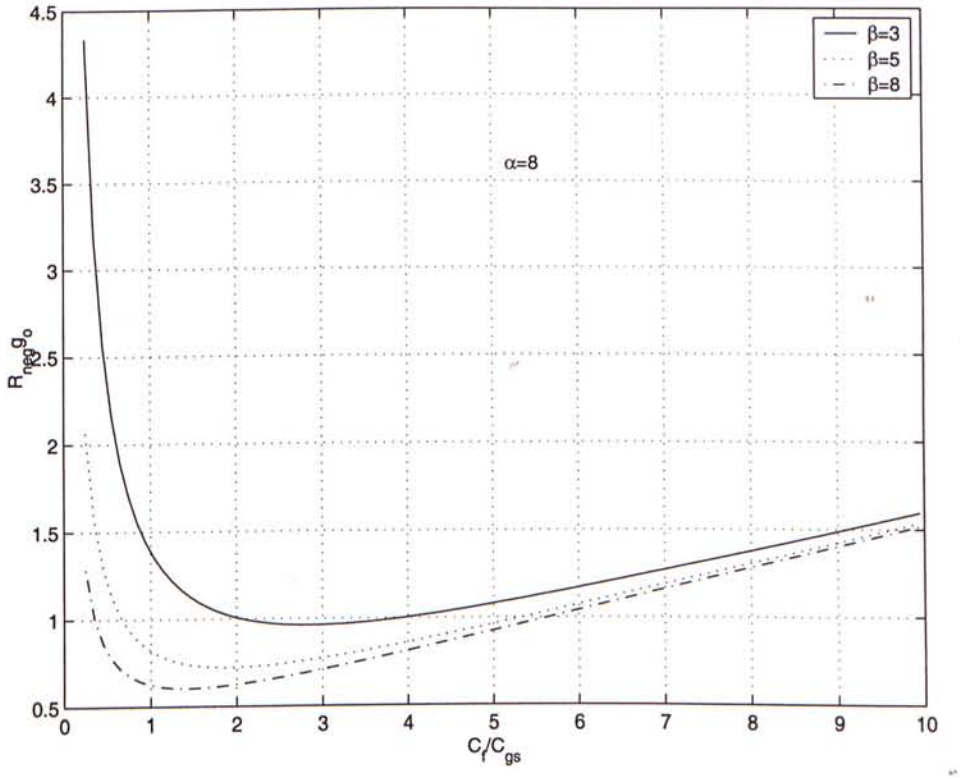

Fig, 3.9 Variations of $R_{neg}g_o$ versus C_f / C_{gs} and β

Chapter 4 Intermodulation Analysis

As the active filter may be used as a band selection filter, the noise and nonlinear behaviors are therefore the main concern of the design. In this section, the nonlinear behavior of the negative resistance circuit is analyzed. This analysis is then extended to the overall active filter. The IMD levels for a second-, a third- and a forth-order active filter are expressed in a closed form.

The IM performances of the active filter are investigated using the Volterra-series formulation [19]. In doing so, the expression of the IMD is derived as a function of the circuit parameters. With the proper choice of circuit component value, the IMD can be reduced by several orders of magnitude.

4.1 IMD of the Negative Resistance Circuit

In order to carry out the two-tone IM analysis of the active filter, the following assumptions have been made.

1. The filter is operated well below saturation. In this weakly nonlinear case, the Volterra series is valid and only non-linear transfer function up to the third-order is retained in the formulation.
2. The MESFET is modeled by a simple equivalent circuit in which the controlled drain current source is the only nonlinear element, as shown in Fig. 4.1. The

drain-to-source current i_{ds} is approximated by

$$i_{ds} = g_{m1} v_{gs} + g_{m2} v_{gs}^2 + g_{m3} v_{gs}^3 \tag{4.1}$$

where g_{m1}, g_{m2}, g_{m3} are the bias-dependent coefficients. Note that the nonlinear effect of the gate-source junction capacitance is usually negligibly small, in comparison with the mixing contributions associated with g_{m3} at a low GHz frequency range.

3. The generation of high-order mixing products caused by the interactions between the nonlinearities of different FET circuits are neglected here. This is justified by the fact that the first-order mixing products $(dc, \omega_1 \pm \omega_2, 2\omega_1, 2\omega_2)$ are very small due to the low shunting impedance of the resonator at these frequencies.

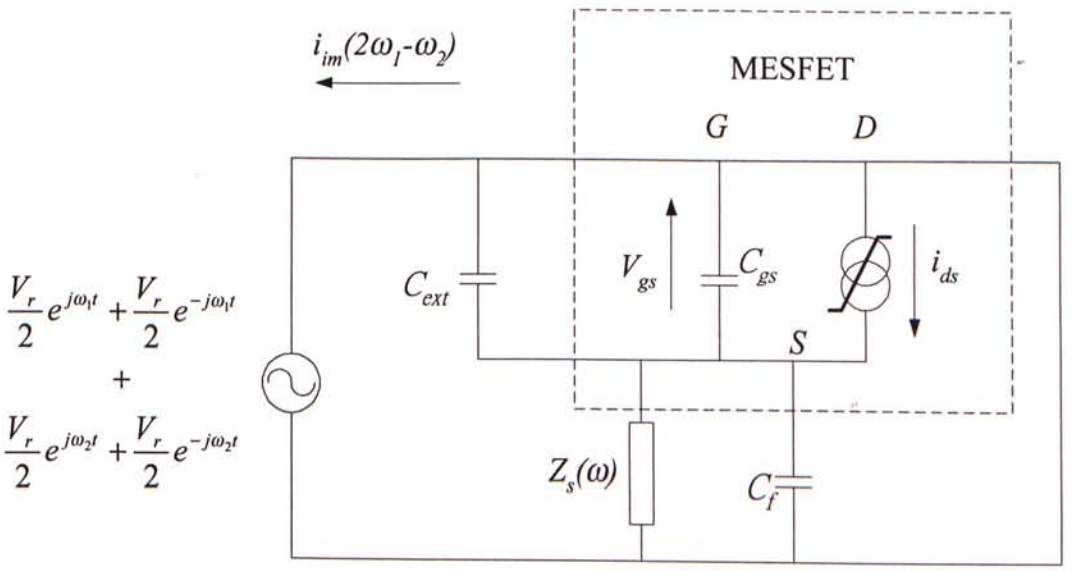

Fig. 4.1 Nonlinear model of negative resistance circuit

By applying the Volterra series concepts and the method of nonlinear currents [9, 19], the following expressions may be derived:

$$i_{im}(2\omega_1-\omega_2)=K_3(2\omega_1-\omega_2)\left[2g_{m2}^2K_2(2\omega_1)+4g_{m2}^2K_2K_2(\omega_1-\omega_2)+3g_{m3}\right]K_1(\omega_1)^2K_1(-\omega_2)\frac{V_r^1V_r^*}{8} \tag{4.2}$$

$$K_1(\omega)=\frac{\frac{C_f}{C_T}}{1+\frac{C_f}{C_T}+\frac{g_{m1}}{j\omega C_T}} \tag{4.3}$$

$$K_2(\omega)=\frac{-1}{g_{m1}+j\omega C_T+j\omega C_f+Y_s(\omega)} \tag{4.4}$$

$$K_3(\omega)=\frac{1}{1+\frac{C_f}{C_T}+\frac{g_{m1}}{j\omega C_T}} \tag{4.5}$$

where $i_{im}(2\omega_1-\omega_2)$ is the IMD currents produced by the nonlinear circuit model. Note that no such information of the phase relationship between the two input signals is required, given the way this problem is formulated. In practice, the third-order mixing term associated g_{m2} is usually less than one-tenth of the term containing g_{m3}. Moreover, as the frequency separation between the two input signal is small $(\omega_1\approx\omega_2\approx\omega_o)$ and $Z_s(\omega)\approx 0$ at low frequencies. Consequently, (4.2) may be simplified as

$$i_{im}(2\omega_1-\omega_2)\approx GV_r^2V_r^*$$

where

$$G=\frac{3g_{m3}}{8}K_1(\omega_o)^2K_1(-\omega_o)K_3(\omega_o) \tag{4.6}$$

Combing (3.9), (4.1) - (4.6), we obtain

$$G=\frac{3g_{m3}}{8}\frac{\left(1+\frac{C_f}{C_T}+j\frac{\alpha}{\beta}\right)^2}{\alpha^3} \tag{4.7}$$

4.2 Analysis of the Active Coupled-Resonator Filter

Fig. 4.2 shows a second-order active coupled-resonator filter. The active *LC*-resonator can be considered as a lossless *LC*-resonator in parallel with a IMD current source, i_{rk} *(k=1,2)*, which is generated by the negative resistance circuits.

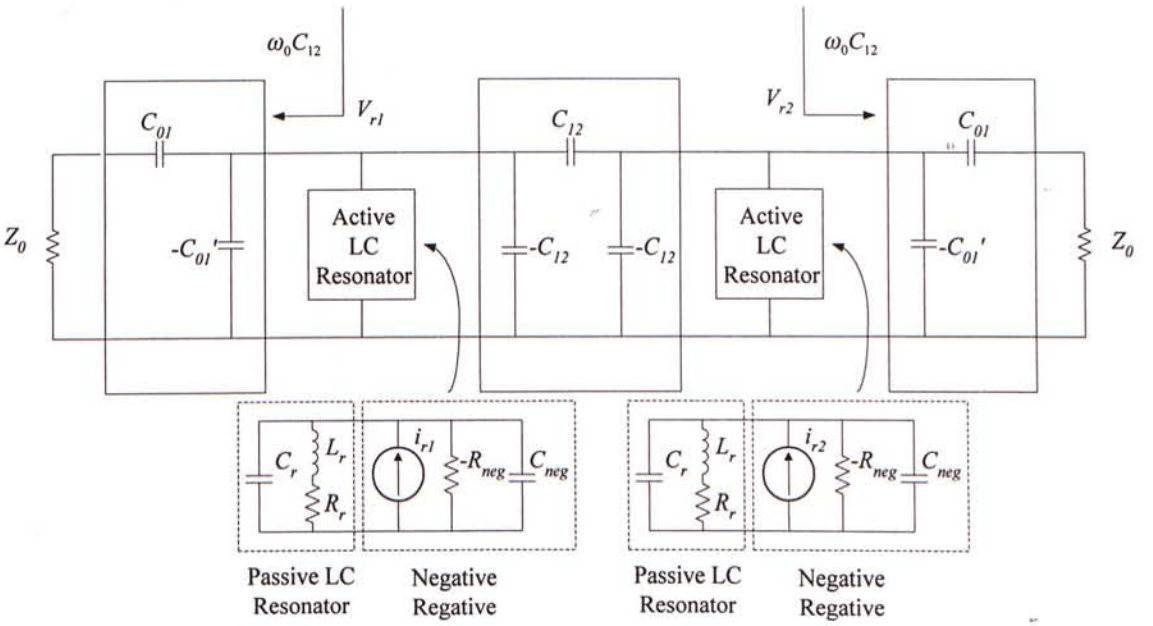

Fig. 4.2 Second-order active filter

When $\omega = \omega_0$, the resonator can be considered as open circuit, and the IMD current flowing through the load by are given by

$$i_{r1o} = \frac{j i_{r1}}{2\omega_0 C_{12}} \frac{j\omega_0 C_{01}}{(1 + j\omega_0 C_{01} Z_0)} \tag{4.8}$$

$$i_{r1o} = \frac{i_{r2}}{2\omega_0 C_{12}} \frac{j\omega_0 C_{01}}{(1 + j\omega_0 C_{01} Z_0)} \tag{4.9}$$

By superposition, the IMD power delivered to the load by the active resonator can be expressed as

$$P_r\big|_{N=2} = \frac{\left|i_{r1o} + i_{r2o}\right|^2}{2} Z_0 = \frac{1}{8\omega_0 C_{12}} \left|ji_{r1} + i_{r2}\right|^2 \tag{4.10}$$

For the third-order active filter, there are three active LC resonators, as well as three current sources, i_{r1}, i_{r2} and i_{r3}. The IMD current flowing through the load are therefore given by

$$i_{r1o} = \frac{-i_{r1}}{2\sqrt{2}\omega_0 C_{12}} \frac{j\omega_0 C_{01}}{(1 + j\omega_0 C_{01} Z_0)} \tag{4.11}$$

$$i_{r2o} = \frac{ji_{r2}}{2\omega_0 C_{12}} \frac{j\omega_0 C_{01}}{(1 + j\omega_0 C_{01} Z_0)} \tag{4.12}$$

$$i_{r3o} = \frac{i_{r3}}{2\sqrt{2}\omega_0 C_{12}} \frac{j\omega_0 C_{01}}{(1 + j\omega_0 C_{01} Z_0)} \tag{4.3}$$

By superposition, the IMD power delivered to the load by the active resonator is

$$P_r\big|_{N=3} = \frac{\left|i_{r1o} + i_{r2o} + i_{r3o}\right|^2}{2} Z_0 = \frac{1}{2}\left|\frac{1}{2\omega_0 C_{12}} \frac{j\omega_0 C_{01}}{(1 + j\omega_0 C_{01} Z_0)}\right|^2 \left|\frac{-i_{r1o} + i_{r3o}}{\sqrt{2}} + ji_{r2o}\right|^2 = \frac{\sqrt{2}}{8\omega_0 C_{12}} \left|\frac{-i_{r1o} + i_{r3o}}{\sqrt{2}} + ji_{r2o}\right|^2 \tag{4.14}$$

Similarly, the forth-order active filter, the IMD current flowing through the load are given by

$$i_{r1o} = \frac{-ji_{r1}}{2\omega_0 \frac{C_{12}^2}{C_{23}}} \frac{j\omega_0 C_{01}}{(1 + j\omega_0 C_{01} Z_0)} \tag{4.15}$$

$$i_{r2o} = \frac{-i_{r2}}{2\omega_0 C_{12}} \frac{j\omega_0 C_{01}}{(1 + j\omega_0 C_{01} Z_0)} \tag{4.16}$$

$$i_{r3o} = \frac{ji_{r3}}{2\omega_0 C_{12}} \frac{j\omega_0 C_{01}}{(1 + j\omega_0 C_{01} Z_0)} \tag{4.17}$$

$$i_{r4o} = \frac{i_{r4}}{2\omega_0 \dfrac{C_{12}^2}{C_{23}}} \frac{j\omega_0 C_{01}}{(1+j\omega_0 C_{01} Z_0)} \tag{4.18}$$

The IMD power delivered to the load by the active resonator is

$$\begin{aligned} P_r\big|_{N=4} &= \frac{\left|i_{r1o} + i_{r2o} + i_{r3o} + i_{r4o}\right|^2}{2} Z_0 \\ &= \frac{1}{2}\left|\frac{j\omega_0 C_{01} Z_0}{2(1+j\omega_0 C_{01} Z_0)}\right|^2 \left|\frac{-ji_{r1} + i_{r4}}{\omega_{0o}\dfrac{C_{12}^2}{C_{23}}} + \frac{-i_{r2} + ji_{r3}}{\omega_0 C_{12}}\right|^2 \\ &= \frac{\omega_0 C_{12}^2}{8C_{23}} \left|\frac{-ji_{r1o} + i_{r4o}}{\omega_0 \dfrac{C_{12}^2}{C_{23}}} + \frac{-i_{r2o} + ji_{r3o}}{\omega_0 C_{12}}\right|^2 \end{aligned} \tag{4.19}$$

4.3 IMD Power of a *N*th-order Active Filter

In section 4.1 and 4.2, the analysis of the IMD power and the active filter has been performed. In this section, we will have the study of the IMD power generated by the overall active filter.

For the second-order active filter, it can be further shown that

$$V_{r2} = jV_{r1} \tag{4.20}$$

$$\left|V_{out}\right|^2 = \frac{\left|V_s\right|^2}{4} \tag{4.21}$$

Combining (4.7) and (4.10), the IMD power delivered to the load of a second-order active filter is

$$
\begin{aligned}
P_{im}(2\omega_1-\omega_2)\big|_{N=2} &= \frac{1}{8\omega_0 C_{12}}\left|jV_{r1}^2V_{r1}^* + V_{r2}^2V_{r2}^*\right|^2|G|^2 \\
&= \frac{1}{2\omega_0 C_{12}}|G|^2|V_{r1}|^6 \\
&= 16\omega_0^4 L_r^4\left(\frac{\omega_0}{BW}\right)^4\left(\frac{3g_{m3}}{8}\right)^2\left(\frac{C_f}{\alpha^2 C_T}\right)^2 P_{in}^3 \\
&= 4\times 2^2\omega_0^4 L_r^4\left(\frac{\omega_0}{BW}\right)^4\left(\frac{3g_{m3}}{8}\right)^2\left(\frac{C_f}{\alpha^2 C_T}\right)^2 P_{in}^3
\end{aligned}
\tag{4.22}
$$

For the third-order active filter,

$$V_{r3} = j\frac{V_{r2}}{\sqrt{2}} = -V_{r1} \tag{4.23}$$

$$V_{r2} = j\sqrt{2}V_{r1} \tag{4.24}$$

$$|V_{r1}|^2 = \frac{|V_s|^2}{4\sqrt{2}\omega_0 C_{12} Z_0} \tag{4.25}$$

where V_{rk} ($k = 1, 2, 3$) is the voltage across the k^{th} resonator

Similarly, the IMD power delivered to the load of a third-order active filter is

$$
\begin{aligned}
P_{im}(2\omega_1-\omega_2)\big|_{N=3} &= \frac{\sqrt{2}}{8\omega_0 C_{12}}\left|\frac{-GV_{r1}^2V_{r1}^* + GV_{r3}^2V_{r3}^*}{\sqrt{2}} + jGV_{r2}^2V_{r2}^*\right|^2 \\
&= \frac{18\sqrt{2}}{8\omega_0 C_{12}}|G|^2|V_{r1}|^6 \\
&= \frac{9\sqrt{2}}{4}\sqrt{2}\omega_0 L_r\frac{\omega_0}{BW}\left(\frac{3g_{m3}}{8}\right)^2\left(\frac{C_f}{\alpha^2 C_T}\right)^2\left(2P_{in}\frac{\omega_0}{BW}\omega_0 L_r\right)^3 \\
&= 36(\omega_0 L_r)^4\left(\frac{\omega_0}{BW}\right)^4\left(\frac{3g_{m3}}{8}\right)^2\left(\frac{C_f}{\alpha^2 C_T}\right)^2 P_{in}^3 \\
&= 4\times 3^2(\omega_0 L_r)^4\left(\frac{\omega_0}{BW}\right)^4\left(\frac{3g_{m3}}{8}\right)^2\left(\frac{C_f}{\alpha^2 C_T}\right)^2 P_{in}^3
\end{aligned}
\tag{4.26}
$$

For the forth-order active filter,

$$V_{r4} = j\frac{C_{23}}{C_{12}}V_{r3} = -\frac{C_{23}}{C_{12}}V_{r2} = -jV_{r1} \tag{4.27}$$

$$V_{r3} = jV_{r2} = -\frac{C_{12}}{C_{23}}V_{r1} \tag{4.28}$$

$$V_{r2} = j\frac{C_{12}}{C_{23}}V_{r1} \tag{4.29}$$

$$|V_{r1}|^2 = \frac{|V_s|^2}{4\omega_0 \frac{C_{12}^2}{C_{23}} Z_0} \tag{4.30}$$

where V_{rk} $(k = 1, 2, 3, 4)$ is the voltage across the k^{th} resonator

The IMD power delivered to the load of a forth-order active filter is

$$P_{im}(2\omega_1 - \omega_2)\big|_{N=4} = \frac{\omega_0 C_{12}^2}{8C_{23}} \left| \frac{-jGV_{r1}^2 V_{r2}^* + GV_{r4}^2 V_{r4}^*}{\frac{\omega_0 C_{12}^2}{C_{23}}} + \frac{-GV_{r2}^2 V_{r2}^* + jGV_{r3}^2 V_{r3}^*}{\omega_0 C_{12}} \right|^2$$

$$= \frac{\omega_0 C_{12}^2}{2C_{23}} |G|^2 |V_{r1}|^6 \left(\frac{1}{\frac{\omega_0 C_{12}^2}{C_{23}}} + \frac{\left(\frac{C_{12}}{C_{23}}\right)^3}{\omega_0 C_{12}} \right)^2$$

$$= \frac{1}{2}\frac{BW}{\omega_0}\frac{1}{\omega_0 L_r g_1} |G|^2 \left(2P_{in}\frac{\omega_0}{BW}\omega_0 L_r g_1 \right)^3 \left(\frac{\omega_0}{BW}\omega_0 L_r \right)^2 \left(g_1 + \frac{g_2^2}{g_1} \right)^2$$

$$= 4g_1^2 \left(g_1 + \frac{g_2^2}{g_1} \right)^2 (\omega_0 L_r)^4 \left(\frac{\omega_0}{BW} \right)^4 \left(\frac{3g_{m3}}{8} \right)^2 \left(\frac{C_f}{\alpha^2 C_T} \right)^2 P_{in}^3$$

$$= 4\times 4^2 (\omega_0 L_r)^4 \left(\frac{\omega_0}{BW} \right)^4 \left(\frac{3g_{m3}}{8} \right)^2 \left(\frac{C_f}{\alpha^2 C_T} \right)^2 P_{in}^3 \tag{4.31}$$

From the above expression of $P_{im}(2\omega_1-\omega_2)$, we can conclude the general expression of the IMD power generated by the N^{th} ($N=2, 3, 4$)-order active filter is

$$P_{im}(2\omega_1-\omega_2)=4\times N^2\omega_0^4 L_r^4\left(\frac{\omega_0}{BW}\right)^4\left(\frac{3g_{m3}}{8}\right)^2\left(\frac{C_f}{\alpha^2 C_T}\right)^2 P_{in}^3 \qquad (4.32)$$

The above expression reveals the influence of device parameters, component values, and the filter characteristic on the IM performance of the filter circuit as follows.

1. The IMD power is directly proportional to the square of the order of the filter.
2. Fig. 4.6 shows the plot of $20\ log(\ C_f\ /\ \alpha^2 C_T)$ as a function of α and β, in combined with (3.11). It can be seen from the diagram that $C_{f(-)}$ should be chosen for low IMD requirements. Furthermore, the IMD level decreases with increasing $\alpha(g_{m1})$ and $\beta(C_T)$ values.
3. Losses within the passive part of the filter, characterized by the inductor Q-factor, have a direct effect on the IM performance. Equation (4.50) indicated that IMD level decreases with increasing Q-factor (decreasing g_o).
4. The bandwidth of the filter has a strong effect on IMD generation (to the forth-power), although the internal voltages within a resonator are only scaled in inverse proportion to its bandwidth.
5. g_{m2} and g_{m3} are bias-dependent coefficients, and it might be possible to further reduce IMD by changing the bias condition of the MESFET device.

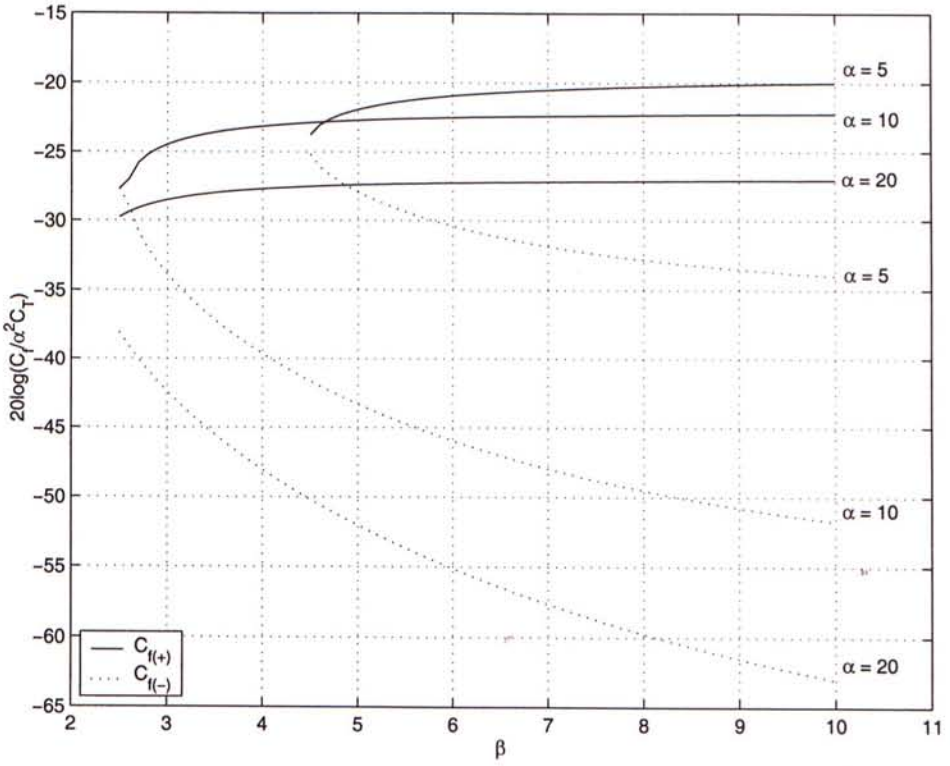

Fig. 4.6 IMD factor as a function of α and β

Chapter 5 Noise Analysis

In this chapter, basic noise theory and the concepts of noise correlation matrix are reviewed. Furthermore, noise parameters extraction of MESFET device by the use of correlation matrix, are also studied. This extraction technique is then used to obtain the noise parameters of CFY30 GaAs MESFET devices.

5.1 Noise Basics and Noise Figure

If the noise voltage (v_n) produced by several identical circuits is measured over a period of time, it is usually found that the measurements at any instant of time, as well as over any time interval, are all different and not related. However, there are some statistical properties that can be measured. It is found that the mean value of such noise is zero while the mean-square value of v_n has a constant value.

$$\overline{v_n} = \lim_{T\to\infty} \frac{1}{T} \int_{t_1}^{t_1+T} v_n(t)dt = 0 \tag{5.1}$$

There are several types of noise produced by microwave devices. The most important is thermal noise. Thermal noise is produced by the random motion of thermally agitated electrons in a conductor. The *rms* value of the thermal noise voltage produced by a resistor R is given by

$$\begin{aligned} v_{n,rms} &= \sqrt{\overline{v_n^2}} \\ &= \sqrt{4kTRB} \end{aligned} \tag{5.2}$$

where k is the Boltzmann constant, T is the absolute temperature and B is the bandwidth. This expression is valid at room temperature for frequencies up to approximately 1THz. Fig. 5.1 shows the two possible equivalent noise models of a noisy resistor.

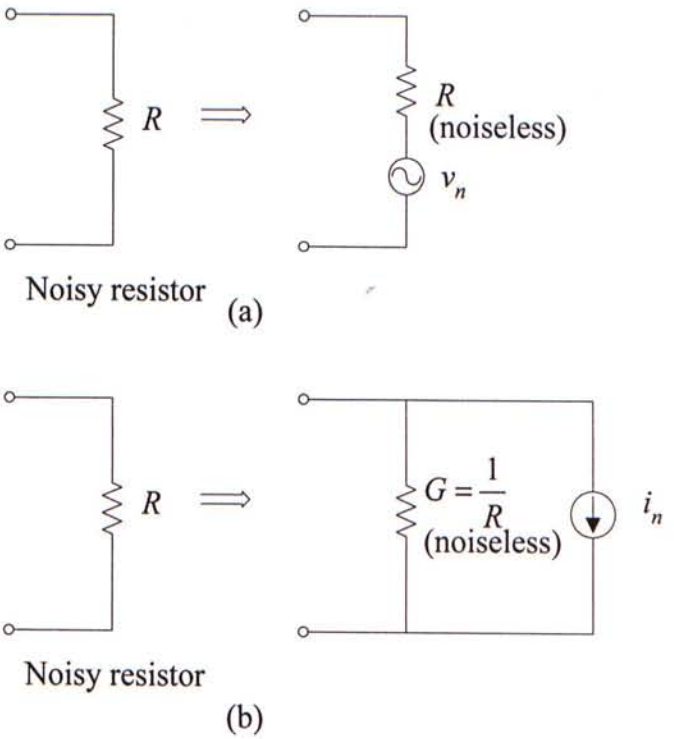

Fig. 5.1 Noise model of resistor: (a) series equivalent; (b) shunt equivalent

Resistance noise occurs in almost all circuits, but reactive elements may alter the frequency density. Fig. 5.2 is a one-port network containing only resistance, capacitance and inductance, and having the equivalent impedance $Z(f) = R(f) + jX(f)$. When the resistances are in thermal equilibrium temperature T, *Nyquist's formula* states that

$$\overline{v_n^2(f)} = 4R(f)kT \tag{5.3}$$

or

$$\overline{i_n^2(f)} = \frac{4kTR(f)}{|Z(f)|^2} \tag{5.4}$$

Hence, the mean square voltage density takes the shape of the equivalent resistance $R(f)$. Equation (5.3) and (5.4) includes the special case of an all-resistive network whose equivalent resistance will be independent of f. Fig. 5.2 shows the noise equivalent circuit of a lossy resonator. The noise generated by a lossy resonator is

$$\begin{aligned} \overline{i_{nr}^2} &= \frac{4kT\,\mathrm{Re}(Z_r)}{|Z_r|^2} \\ &= \frac{4kTR_r}{R_r^2 + \omega^2 L_r^2} \\ &\approx 4kTg_o \end{aligned} \tag{5.5}$$

where

$$Z_r = \frac{1}{\dfrac{1}{j\omega L_r + R_r} + j\omega C_r}$$

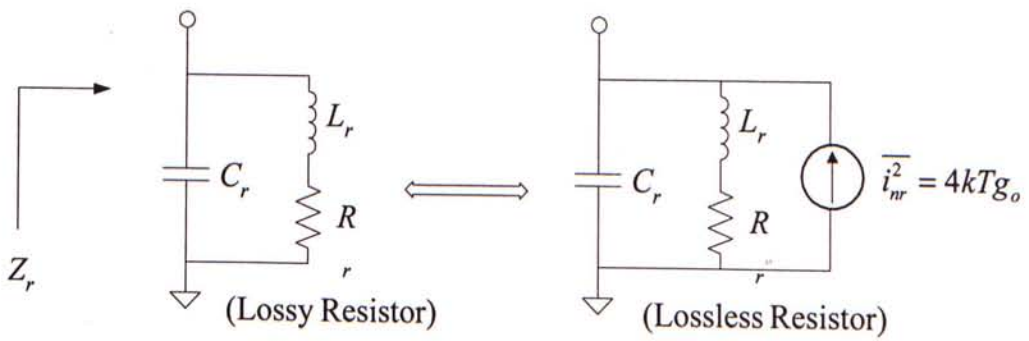

Fig. 5.2 Noise generated by the resonator

Next, we consider the noise characteristic of a noisy two-port network. A noisy two-port network is shown in Fig. 5.3, where the available input noise power from the resistor R_s is $P_{Ni}=kTB$. This input noise power gets amplified by the available gain of

the two-port network (G_A) and appears at the output. In addition, the noisy two-port network contributes a certain amount of noise power to the output. The total available noise power at the output is

$$\begin{aligned} P_{No} &= G_A P_{Ni} + P_n \\ &= G_A kTB + P_n \end{aligned} \tag{5.6}$$

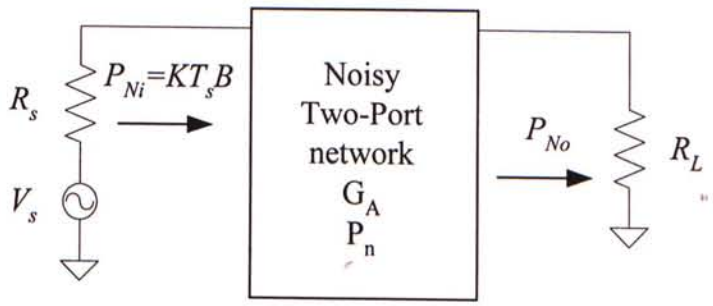

Fig. 5.3 Noisy two-port network

G_A can be expressed in the form

$$G_A = \frac{P_{so}}{P_{si}} \tag{5.7}$$

where P_{so} is the available signal power at the output and P_{si} is the available signal power at the input. The noise figure F of a two-port network at a specific signal frequency is defined as

$$\begin{aligned} F &= \frac{P_{Si}/P_{Ni}}{P_{So}/P_{No}} \\ &= \frac{P_{No}}{G_A P_{Ni}} \\ &= 1 + \frac{P_n}{G_A P_{Ni}} \end{aligned} \tag{5.8}$$

5.2 Noisy Two-Ports

The circuit theory of linear noisy network shows that any noisy two-port can be replaced by a noise equivalent circuit which consists of the original two-port (assumed to be noiseless) and two additional noise sources [20], as shown in Fig.5.4. The admittance representation uses two current noise sources i_{n1} and i_{n2}, the impedance representation uses two voltage noise sources v_{n1} and v_{n2} and the chain representation uses a voltage noise source v_n and a current noise source i_n.

The electrical behavior of these noisy two-ports can be described by two linear equations between the input voltage and current v_1 and i_1 and the output voltage and current v_2 and i_2. For Fig. 5.5a,

$$v_1 = z_{11}i_1 + z_{12}i_2 + v_{n1} \tag{5.9}$$

and

$$v_2 = z_{21}i_1 + z_{22}i_2 + v_{n2} \tag{5.10}$$

For Fig. 5.5b,

$$i_1 = y_{11}v_1 + y_{12}y_2 + i_{n1} \tag{5.11}$$

and

$$i_2 = y_{21}v_1 + y_{22}v_2 + i_{n2} \tag{5.12}$$

For Fig. 5.5c,

$$i_1 = Av_1 + Bi_2 + i_n \tag{5.13}$$

and

$$v_2 = Cv_2 + Di_2 + v_n \tag{5.14}$$

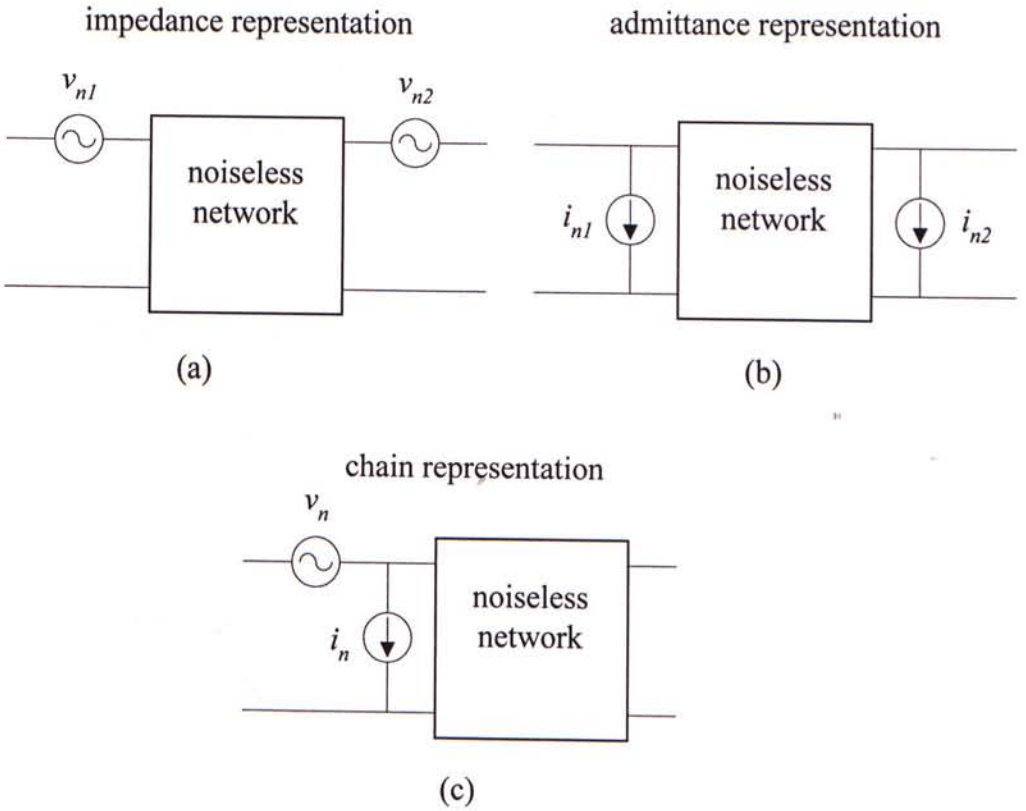

Fig. 5.4 Different representation of noisy two-port network

A source connected to the noisy two-port network is shown in Fig. 5.5. The source is represented by a current source with admittance Y_s. The noise from the source and the noise from the two-port network are assumed to be uncorrelated. As the total noise power is proportional to the mean square of the short-circuit current at the input port of the noise free two-port network, the noise figure of the noisy network is given by

$$F = 1 + \frac{\overline{(i_n + v_n Y_s)^2}}{\overline{i_s^2}} \tag{5.15}$$

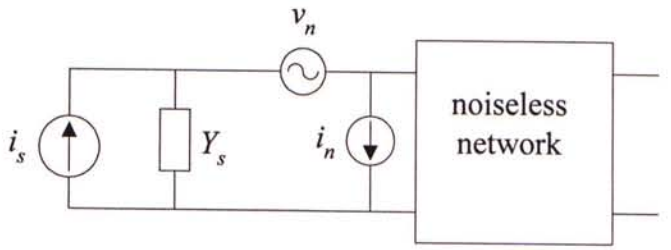

Fig. 5.5 Noise model for calculation of the two-port network noise figure

As there is some correlation between the noise sources v_n and i_n. i_n can be written in terms of two parts; one part is uncorrelated to v_n (called i_{nu}), and the other part is correlated to v_n (called i_{nc}). Thus

$$i_n = i_{nu} + i_{nc} \tag{5.16}$$

Furthermore, the relation between i_{nc} and v_n can be defined in terms of a correlation admittance Y_c,

$$i_{nc} = Y_c v_n \tag{5.17}$$

It can be shown that the minimum noise figure, F_{min}, can be obtained when the noisy two-port is matched with optimum source admittance, Y_{opt}. The expression for the minimum noise figure and the optimum source admittance are

$$F_{\min} = 1 + 2R_N\left(G_{opt} + G_c\right) \tag{5.18}$$

$$\begin{aligned} Y_{opt} &= G_{opt} + jB_{opt} \\ &= \sqrt{G_c^2 + \frac{G_u}{R_N}} - jB_c \end{aligned} \tag{5.19}$$

where

$$R_N = \frac{\overline{v_n^2}}{4KT_oB}$$

$$G_u = \frac{\overline{i_{nu}^2}}{4kTB}$$

$$Y_c = G_c + jB_c$$

In general, the noise characteristic of a noisy two-port can be characterized by the three noise parameters,

1. Minimum noise figure, F_{min},
2. Noise resistance, R_N,
3. Optimum source admittance, Y_{opt}.

5.3 Correlation Matrix Representation of Noisy Two-Ports

When the noisy two-port is replaced by a noise equivalent circuit which consists of the original two-port and two additional noise sources, a physical significant description of these sources is given by their self- and cross-power spectral densities which are defined as Fourier transform of their auto and cross-correlation functions, Fig. 5.6. Arranging these spectral densities in matrix form leads to the correlation matrices [21].

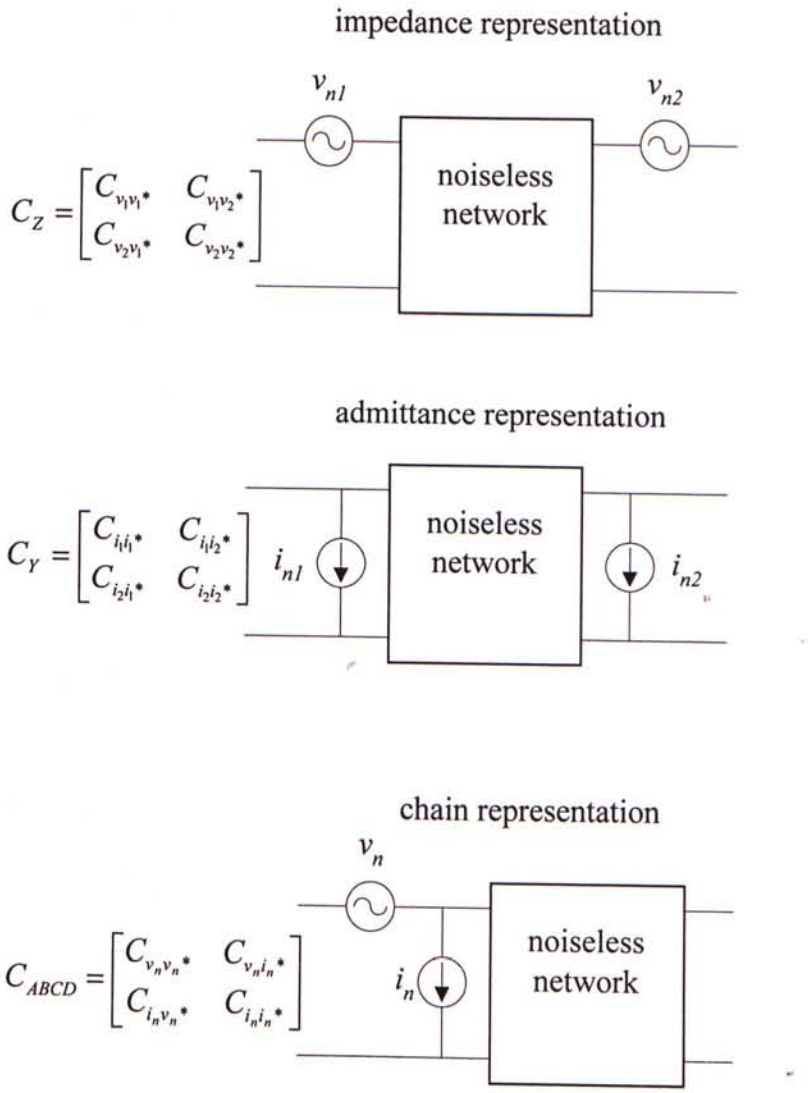

Fig. 5.6 Correlation matrices of different representations

The elements of matrices are denoted by $C_{s_1s_2^*}$ where the subscript indicates that the spectral density refers to the noise source s_1 and s_2. The noiseless part of the noise equivalent two-port is described by electrical matrix. These matrices are the conventional two-port matrices.

Noise sources are usually characterized by their mean fluctuation in bandwidth Δf centered on frequency f. For two noise source s_1 and s_2, the mean fluctuations are $\langle s_1 s_1^* \rangle$, $\langle s_1 s_2^* \rangle$, $\langle s_2 s_1^* \rangle$ and $\langle s_2 s_2^* \rangle$ where $\langle s_i s_j^* \rangle$ denotes the mean fluctuation of

a product containing the signal s_i and the complex conjugate of the signal s_j. Mean fluctuations are closely related to power spectral densities by the relation,

$$\left\langle s_i s_j^* \right\rangle = 2\Delta f C_{s_i s_j} \qquad i, j = 1,2 \tag{5.20}$$

The factor 2 occurs because the frequency range has been taken from $-\infty$ to $+\infty$. The correlation matrix C belonging to the noise source s_1 and s_2 can then be written as

$$C = \frac{1}{2\Delta f}\begin{bmatrix} \left\langle s_1 s_1^* \right\rangle & \left\langle s_1 s_2^* \right\rangle \\ \left\langle s_2 s_1^* \right\rangle & \left\langle s_2 s_2^* \right\rangle \end{bmatrix} \tag{5.21}$$

5.4 Change of Representation

The representation can be transformed into each other by simple transformation operations

$$C' = TCT^+ \tag{5.22}$$

where C and C' denote the correlation matrix of the original and resulting representation, respectively and T is the transformation matrix. The sign (+) is used to denote Hermitian conjugation. A set of matrices covering all possible transformations between impedance, admittance and chain representation is presented in Table 5.1.

		original representation		
		admittance	impedance	chain
resulting representation	admittance	$\begin{bmatrix} 1 & 0 \\ 0 & 1 \end{bmatrix}$	$\begin{bmatrix} y_{11} & y_{12} \\ y_{21} & y_{22} \end{bmatrix}$	$\begin{bmatrix} -y_{11} & 1 \\ -y_{21} & 0 \end{bmatrix}$
	impedance	$\begin{bmatrix} z_{11} & z_{12} \\ z_{21} & z_{22} \end{bmatrix}$	$\begin{bmatrix} 1 & 0 \\ 0 & 1 \end{bmatrix}$	$\begin{bmatrix} 1 & -z_{11} \\ 0 & -z_{21} \end{bmatrix}$
	chain	$\begin{bmatrix} 0 & B \\ 1 & D \end{bmatrix}$	$\begin{bmatrix} 0 & -A \\ 1 & -C \end{bmatrix}$	$\begin{bmatrix} 1 & 0 \\ 0 & 1 \end{bmatrix}$

Table 5.1. Transformation Matrices

5.5 Interconnection of Noisy Two-Ports

For applications in noise analysis, interconnections of two-ports either in parallel, in series or in cascade are of particular interest. For these interconnections the resulting correlation matrix is related to the correlation matrices of the original two-ports by

$$C_Y = C_{Y_1} + C_{Y_2} \qquad \text{(parallel)} \tag{5.23}$$

$$C_Z = C_{Z_1} + C_{Z_2} \qquad \text{(series)} \tag{5.24}$$

$$C_A = A_1 C_{A_2} A_1^+ + C_{A_1} \qquad \text{(cascade)} \tag{5.25}$$

where the subscripts 1 and 2 refer to the two-ports to be connected. As shown by

these equations, interconnection in parallel and in series corresponds to addition of the correlation matrices in admittance and impedance representation, respectively. For cascading, a more complicated relation is obtained which additionally contains the electrical matrix A_1 of the first two-port.

5.6 Correlation Matrix of the Basic Two-Ports

The two-port analysis starts from basic two-ports whose correlation matrices have to be known. These matrices are obtained from either theoretical considerations or noise measurements. An important example belonging to the former case is the thermal noise of two-ports consisting only of passive matrices. The correlation matrices in impedance and admittance representation of such a two-port are

$$C_Z = 2kT\,\mathrm{Re}\{Z\} \tag{5.26}$$

$$C_Y = 2kT\,\mathrm{Re}\{Y\} \tag{5.27}$$

They are completely determined by the temperature T and the real part of their electrical matrices in impedance and admittance representation, respectively.

Theoretical estimations of the correlation matrix can be obtained if noise equivalent circuits of the elements are used. This is demonstrated by a simplified MESFET model as depicted in Fig. 5.7. The model contains two noise current, namely i_g and i_d.

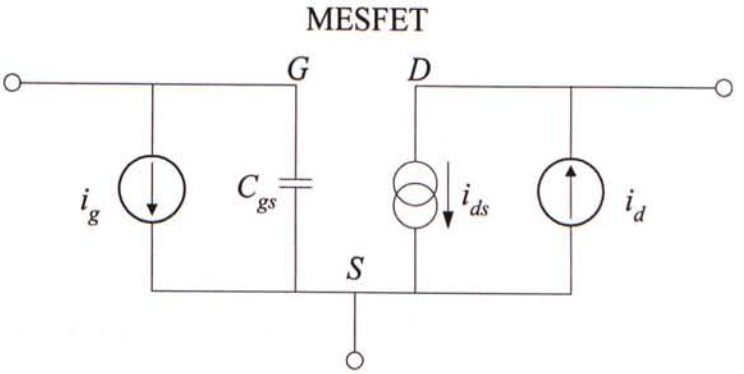

Fig. 5.7 Simplified intrinsic noise circuit of MESFET

The correlation matrix of the intrinsic MESFET is according to (5.21)

$$C_Y = \frac{1}{2\Delta f}\begin{bmatrix} \langle i_g i_g^* \rangle & \langle i_g i_d^* \rangle \\ \langle i_d i_g^* \rangle & \langle i_d i_d^* \rangle \end{bmatrix} \tag{5.28}$$

Following van der Ziel [22], [23] and [24] the noise current source, $\overline{i_g^2}$ and $\overline{i_d^2}$ can be expressed as

$$\overline{i_g^2} = \frac{4kT\Delta f(\omega C_{gs})^2 R}{gm} \tag{5.29}$$

$$\overline{i_d^2} = 4kTg_m\Delta fP \tag{5.30}$$

where R and P are dimensionless parameters depending upon the technological parameters and biasing conditions. The correlation coefficient of the two current source are defined by

$$C = \frac{\overline{i_g^* i_d}}{j\sqrt{\overline{i_g^2 i_d^2}}} \tag{5.31}$$

Note that these parameters, P, R and C are frequency independent.

Thus, equation (5.28) can be rewritten as

$$C_Y = \frac{1}{2\Delta f}\begin{bmatrix} \frac{R(\omega C_{gs})^2}{g_m} & -j\omega C C_{gs}\sqrt{PR} \\ j\omega C C_{gs}\sqrt{PR} & Pg_m \end{bmatrix} \tag{5.32}$$

However, a practical MESFET usually consists of parasitics in its terminals. It can be considered as three noisy two-port connected in series as shown in Fig. 5.8. For gate-drain parasitics, the electrical (Z_{GD}) and correlation matrices (C_{GD}) is given by

$$Z_{GD} = \begin{bmatrix} R_g + j\omega L_g & 0 \\ 0 & R_d + j\omega L_d \end{bmatrix} \tag{5.33}$$

$$C_{GD} = 2kT\begin{bmatrix} R_g & 0 \\ 0 & R_d \end{bmatrix} \tag{5.34}$$

For source parasitics, the electrical (Z_S) and correlation (C_S) matrices is given by

$$Z_{Ss} = \begin{bmatrix} R_s + j\omega L_s & R_s + j\omega L_s \\ R_s + j\omega L_s & R_s + j\omega L_s \end{bmatrix} \tag{5.35}$$

$$C_S = \begin{bmatrix} R_s & R_s \\ R_s & R_s \end{bmatrix} \tag{5.36}$$

The impedance representation of correlation matrix of the overall transistor is

$$C_{FET,Z} = C_{GD} + C_Z + C_S \tag{5.37}$$

where C_Z is the impedance representation of the correlation matrix of the intrinsic MESFET.

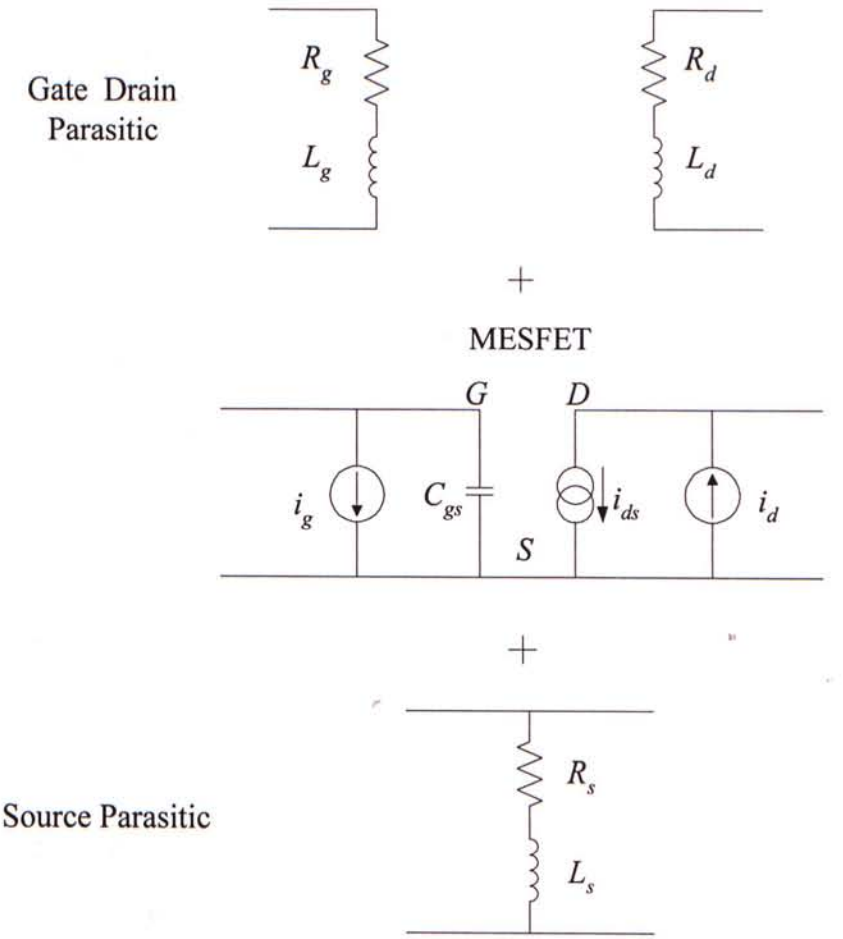

Fig. 5.8 Series connections of the intrinsic MESFET and the parasitic elements

5.7 Extraction of the Noise Parameters of MESFET

As mentioned before, the noise characteristic of the MESFET is generally characterized by F_{min}, R_N and Y_{opt}. The measurement of the intrinsic noise current source of the MESFET is less well developed. A matrix-based noise-parameter extraction technique for MESFET is introduced in the following section [25]. This technique analytically extracts the FET current noise-parameters (P, R and C) from the measured S-parameters and noise parameters and is similar to existing S-parameter techniques in that it removes the device parasitics using the appropriate

matrix forms and finally yields a set of *Y*-parameter based matrices which can be directly solved for the model component and noise-parameter values. The set of matrices consists of a component matrix and a noise correlation matrix. The terminal parasitic resistances and inductances are the only components not determined within this procedure. With reference to Fig. 5.9, the extraction procedure can be summarized as follows:

1. Measure the *S*-parameters and the noise parameters R_N, Y_{opt} and NF_{min} of the MESFET and convert the noise parameters to an *ABCD* correlation matrix C_{ABCD} which is given by

$$C_{ABCD} = 2kT \begin{bmatrix} R_n & \frac{NF_{\min} - 1}{2} - R_n Y_{opt}^* \\ \frac{NF_{\min} - 1}{2} - R_n Y_{opt} & R_n \left| Y_{opt} \right|^2 \end{bmatrix} \tag{5.38}$$

2. Transform the *ABCD* correlation matrix to a *Z* correlation matrix C_Z;

3. Transform *S*-parameters to *Z*-parameters.

4. De-embed series parasitic elements from C_Z and *Z*.

5. Invert the de-embedded *Z* matrix to get a intrinsic *Y* matrix.

6. Use this intrinsic *Y* matrix to transform C_Z to $C_{Y,int}$.

7. It can be seen that the *P*, *R* and *C* parameters are readily determined from the following expressions:

$$P = \frac{\mathrm{Re}\left(C_{y_{\mathrm{int}}2,2}\right)}{g_m} \tag{5.39}$$

$$R = \frac{\mathrm{Re}\left(C_{y_{\mathrm{int}}1,1}\right) g_m}{\left(\omega C_{gs}\right)^2} \tag{5.40}$$

$$C = \frac{-\mathrm{Im}\left(C_{y_{\mathrm{int}}2,1}\right)}{\omega C_{gs}\sqrt{PR}} \tag{5.41}$$

Note that negative sign is given in C as the direction of noise current i_d is defined in an opposite direction of i_g in the admittance representation.

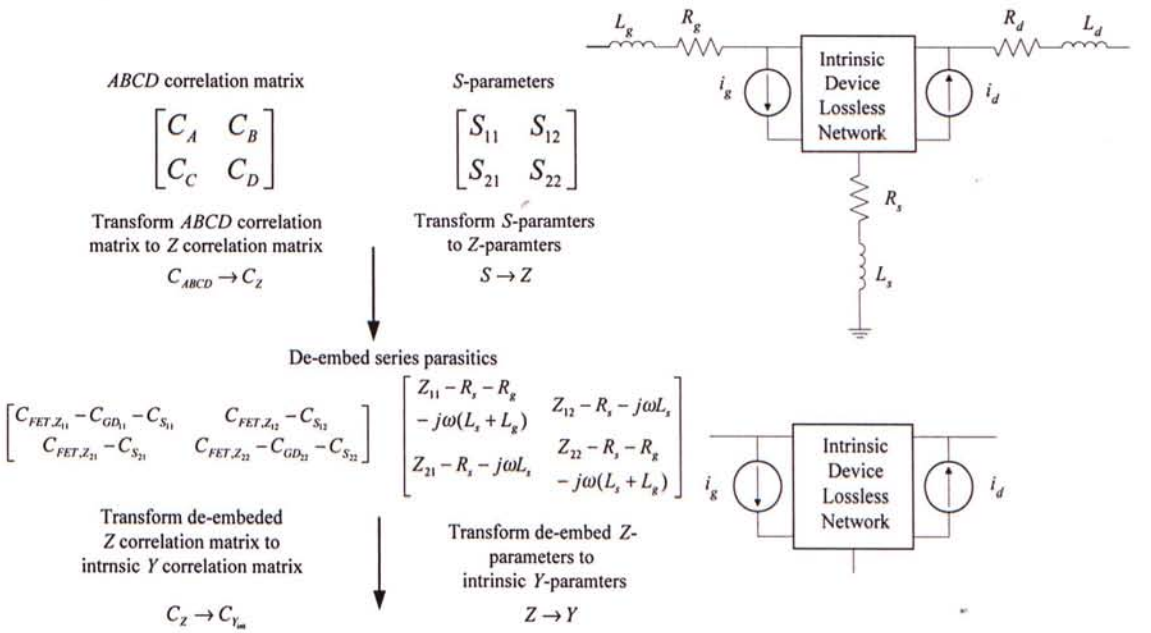

Fig. 5.9.Computation of intrinsic noise parameters

5.8 Noise Parameters of CFY30

The noise parameters of the GaAs MESFET with part number CFY 30 from Siemens is extracted by the above technique. The *S*-parameters and noise parameters of CFY30 are listed in table 5.2 at 2GHz. The values of parasitics of CFY30, obtained by [26], are listed in table 5.3. Furthermore, the value of P, R and C are quoted in table 5.4.

F_{min} / dB	R_N / Ω	Γ_{opt}	S_{11}	S_{21}	S_{12}	S_{22}
1	49	$0.72\angle 27$	$0.96\angle -36$	$2.45\angle 137$	$0.05\angle 60$	$0.65\angle -26$

Table 5.2 *S*-parameters and noise parameters of CFY30 at 2GHz

L_g / nH	R_g / Ω	L_d / nH	R_d / Ω	L_s / nH	R_s / Ω
0.6898	4.7	0.8517	4.666	0.1075	4.252

Table 5.3 Parasitics of CFY30

P	R	C
1.7347	0.54709	0.27707

Table 5.4 Calculated noise parameters of CFY30

A sensitivity study has also been performed to investigate the variations of the extracted noise parameters due to the uncertainties in device parasitics and noise data. Each parasitic element is varied by $\pm 50\%$ and each noise parameter is varied by $\pm 10\%$ for sensitivity evaluation. The results are plotted in Fig. 5.10 and Fig. 5.11.

From Fig. 5.10, we can see that the parasitic element has little effect on the noise parameters. From Fig. 5.11, the parameters are relatively insensitive to variation in F_{min}. However, variation in R_N are found to cause errors in P and R, but not C. Uncertainties in $|\Gamma_{opt}|$ cause significant variations in C and R. Error in the phase of $|\Gamma_{opt}|$ introduce variations in R and C, but not in P.

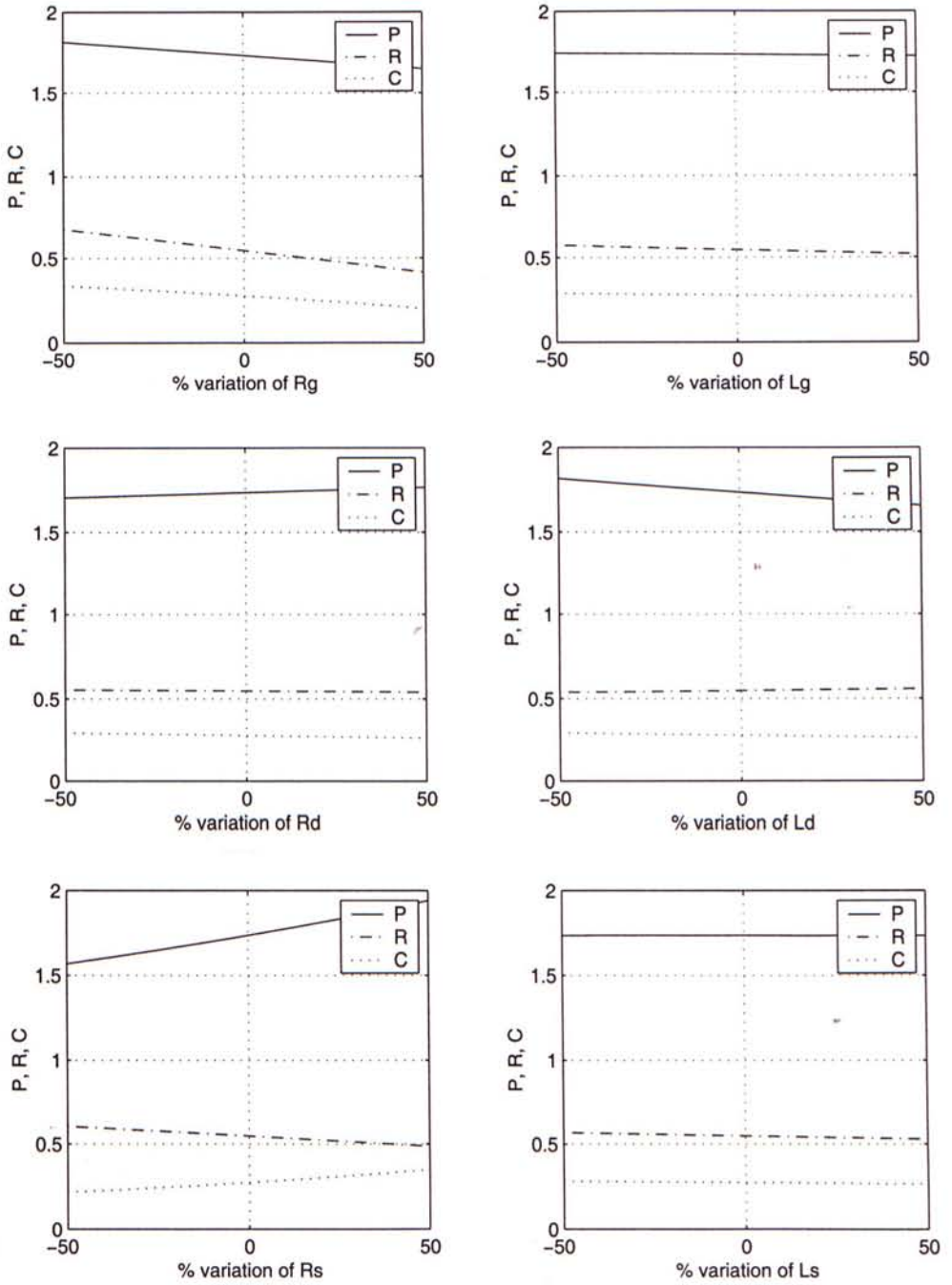

Fig.5.10 Variation of P, R, C versus parasitic elements

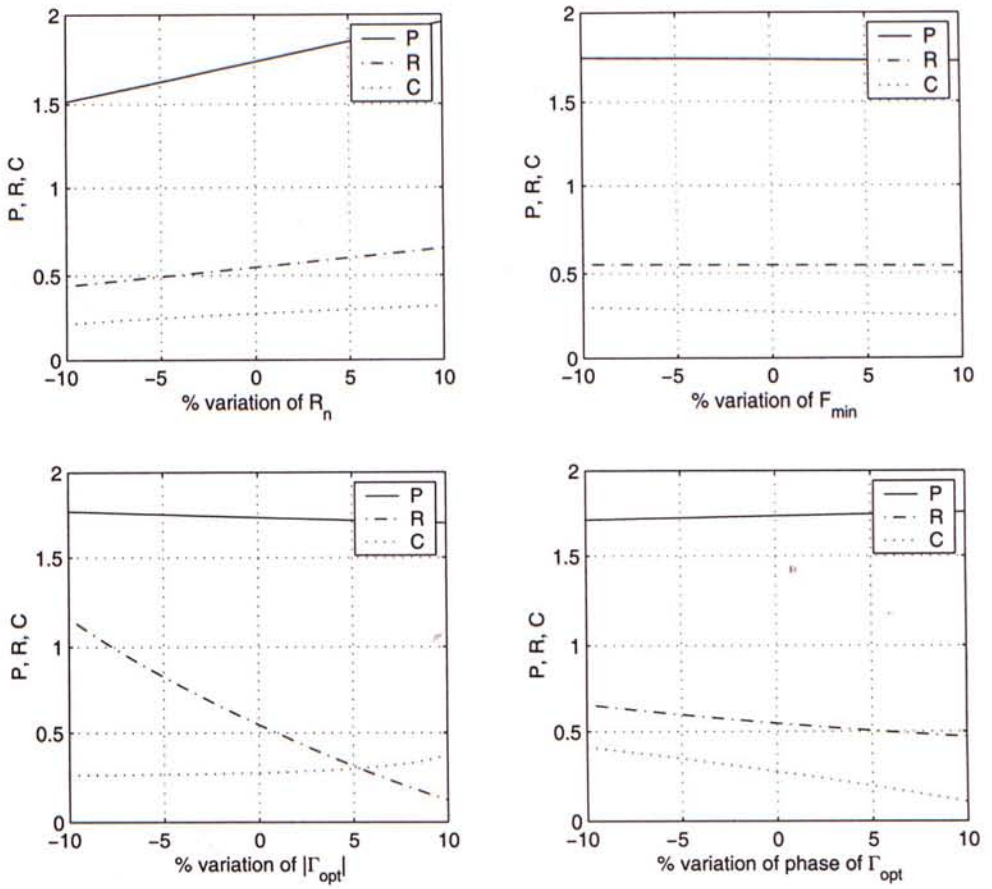

Fig. 5.11 Variation of *P*, *R*, *C* versus noise parameters

5.9 Noise Figure of CFY30

In this session, the noise figure of an unmatched MESFET is evaluated using the noise parameters extracted previously and compared with those obtained from experiment.

The setup shown in Fig. 5.12 is used to measure the noise figure of CFY30. The CFY30 is terminated by a 50Ω load and a noise source with an input impedance of 50Ω. The noise figure of the CFY30 is measured from 500MHz to 2GHz at four

different current levels (5, 10, 20, 30mA) and the results are plotted in Fig. 5.13. The noise figure tends to increase with frequency at all current levels, as expected.

With the help of Fig. 5.14, the noise figure of an unmatched device can be calculated by the following steps.

1. Obtain the intrinsic Y correlation matrix by using P, R and C from table5.4.
2. Calculate the extrinsic Z-parameters at a given frequency, e.g. 1GHz
3. Determine the intrinsic Z-parameters Z_{int} by de-embedding procedure.
4. Transform the intrinsic Y correlation matrix to intrinsic Z correlation matrix by using Z_{int}.
5. Find the extrinsic Z correlation matrix by combing intrinsic Z correlation with parasitics.
6. Transform the extrinsic Z correlation matrix to extrinsic $ABCD$ correlation matrix.
7. Finally, the noise figure of the unmatched device can be obtained as,

$$\begin{aligned} F &= 1 + \frac{\overline{(i_n + v_n Y_0)^2}}{\overline{i_s^2}} \\ &= 1 + \frac{\overline{i_n^2} + \overline{v_n^2} Y_0^2 + \overline{i_n^* v_n} Y_0 + \overline{i_n v_n^*} Y_0}{4kTY_0} \\ &= 1 + \frac{C_{A2,2} + C_{A1,1} Y_0^2 + (C_{A1,2} + C_{A2,1}) Y_0}{4kTY_0} \end{aligned} \tag{5.42}$$

Using the above expression, the noise figure of CFY30 biased at I_d = 15mA is found

to be approximately 3.24dB, which is quite close to the measured data (Fig. 5.14).

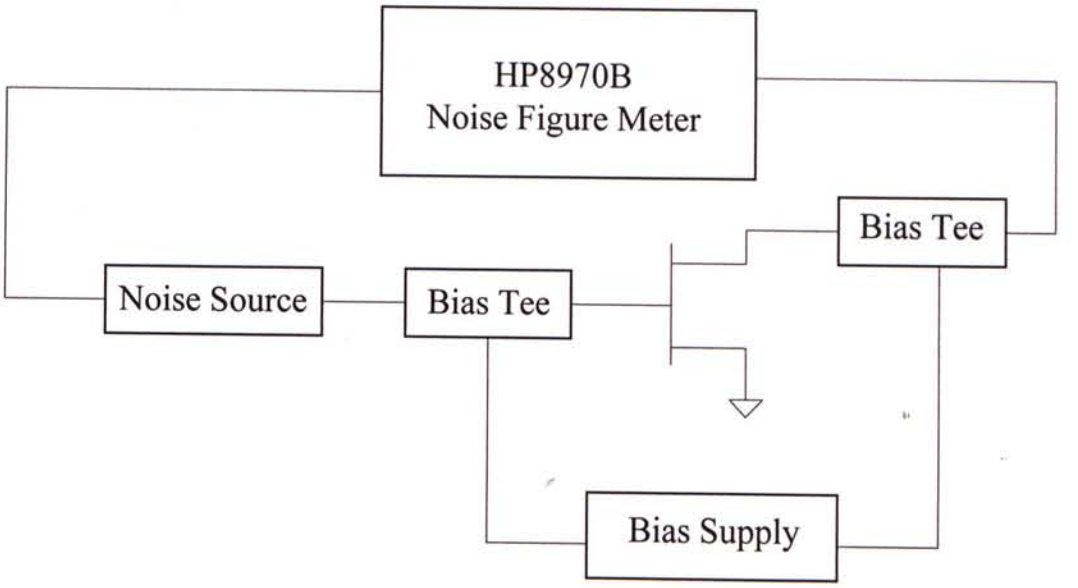

Fig. 5.12 Noise figure measurement configuration

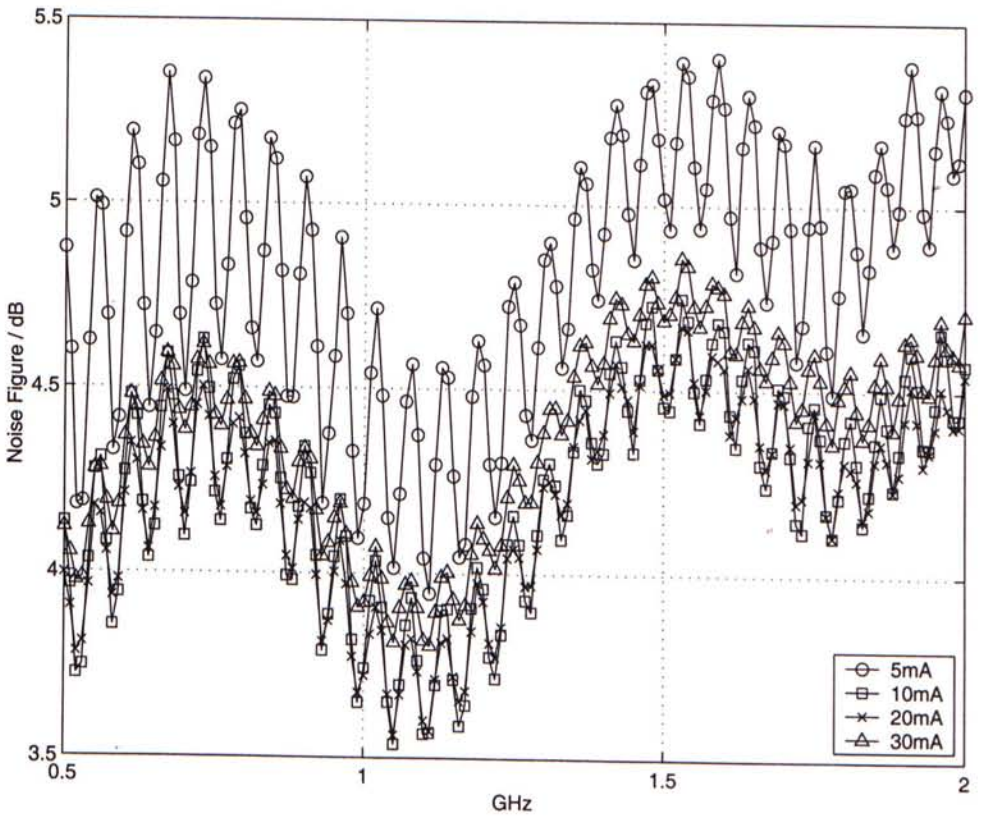

Fig. 5.13 Measured noise figure of CFY30

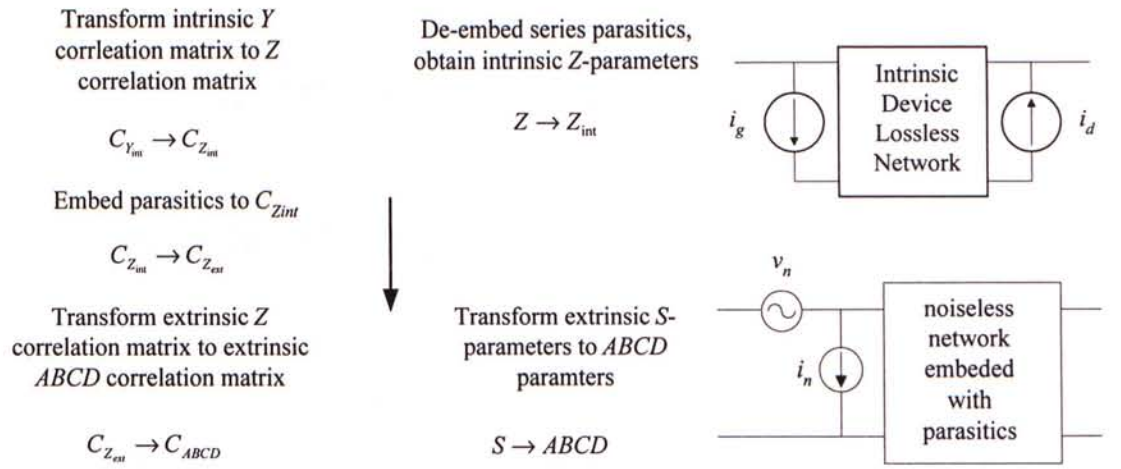

Fig. 5.14 Computation of the extrinsic noise parameter of CFY30

Chapter 6 Noise Analysis of the Passive and Active Filter

In chapter 5, the noise model of the MESFET has been studied and the noise parameters of the MESFET, CFY30 has been extracted. In this chapter, the noise parameters will be used to analysis the noise behavior of the active filter. Furthermore, a simple method will be introduced to optimize the noise figure. A systematic procedures for designing active filters with optimized linearity and noise performance is also presented.

6.1 Noise Current Generated by the Negative Resistance Circuit

Fig. 6.1 shows the simplified noise equivalent circuit of the negative resistance circuit. i_g and i_d are given by (5.30) and (5.31) respectively.

The voltage at node S is

$$v_s = \frac{i_g + v_{gs} j\omega C_T + g_m v_{gs} - i_d}{j\omega C_f}$$

As $v_{gs} = -v_s$

$$v_{gs} = \frac{i_d - i_g}{j\omega C_T + j\omega C_f + g_m}$$

$$i_n = -i_g - v_{gs} j\omega C_T \tag{6.1}$$

$$= \frac{-i_g\left(j\omega C_f + g_m\right) - i_d j\omega C_T}{j\omega C_T + j\omega C_f + g_m}$$

Combining (6.1) with (3.9), i_n can be rewritten as

$$i_n = -\frac{i_g\left(\frac{C_f}{C_T} + \frac{g_m}{j\omega C_T}\right) + i_d}{1 + \frac{C_f}{C_T} + \frac{g_m}{j\omega C_T}} \tag{6.2}$$

$$\overline{i_n^2} = \frac{\overline{i_g^2}\left[\left(\frac{C_f}{C_T}\right)^2 + \left(\frac{\alpha}{\beta}\right)^2\right] + \overline{i_d^2} - 2cor\frac{\alpha}{\beta}}{\alpha\frac{C_f}{C_T}} \tag{6.3}$$

$$= \frac{\overline{i_g^2}\left[\frac{C_f}{C_T}(\alpha - 2) - 1\right] + \overline{i_d^2} - 2cor\frac{\alpha}{\beta}}{\alpha\frac{C_f}{C_T}}$$

where

$$jcor = \overline{i_g^* i_d} = jC\sqrt{\overline{i_g^2}\,\overline{i_d^2}}$$

Fig. 6.2 shows the plot of $10\log\left(\overline{i_n^2}\right)$ as a function of α and β, in combined with (3.11) and P, R, C values in table 5.4 are used. It can be seen that from the diagram that $C_{f(+)}$ should be chosen for low noise current generated by the negative resistance circuit. Furthermore, the noise current decreases with increasing α. β has little effect on the noise current when $C_{f(+)}$ is chosen. On the other hand, β has a strong effect on

the noise current when $C_{f(-)}$ is selected.

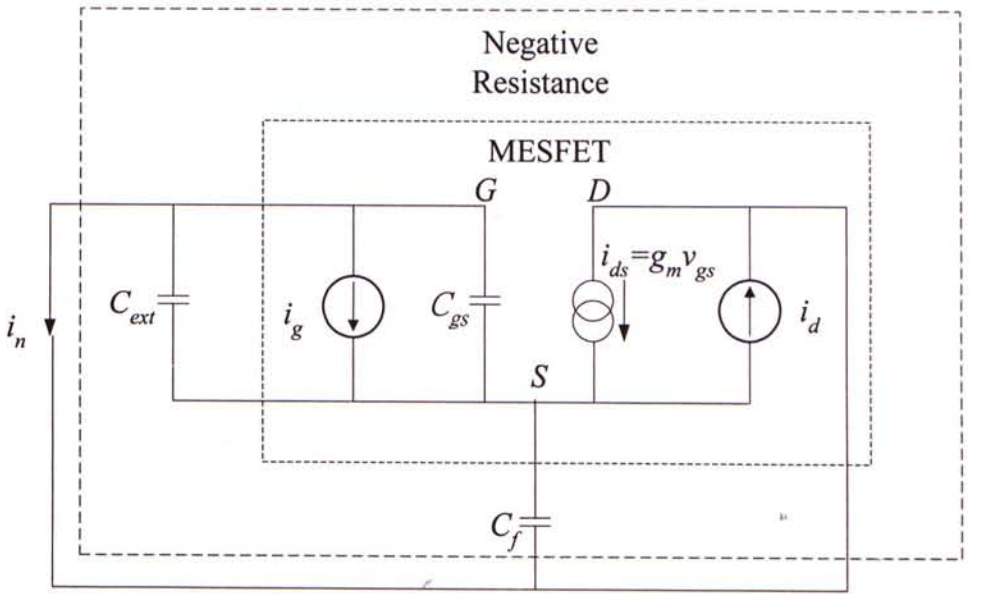

Fig. 6.1 Noise model of the negative resistance circuit

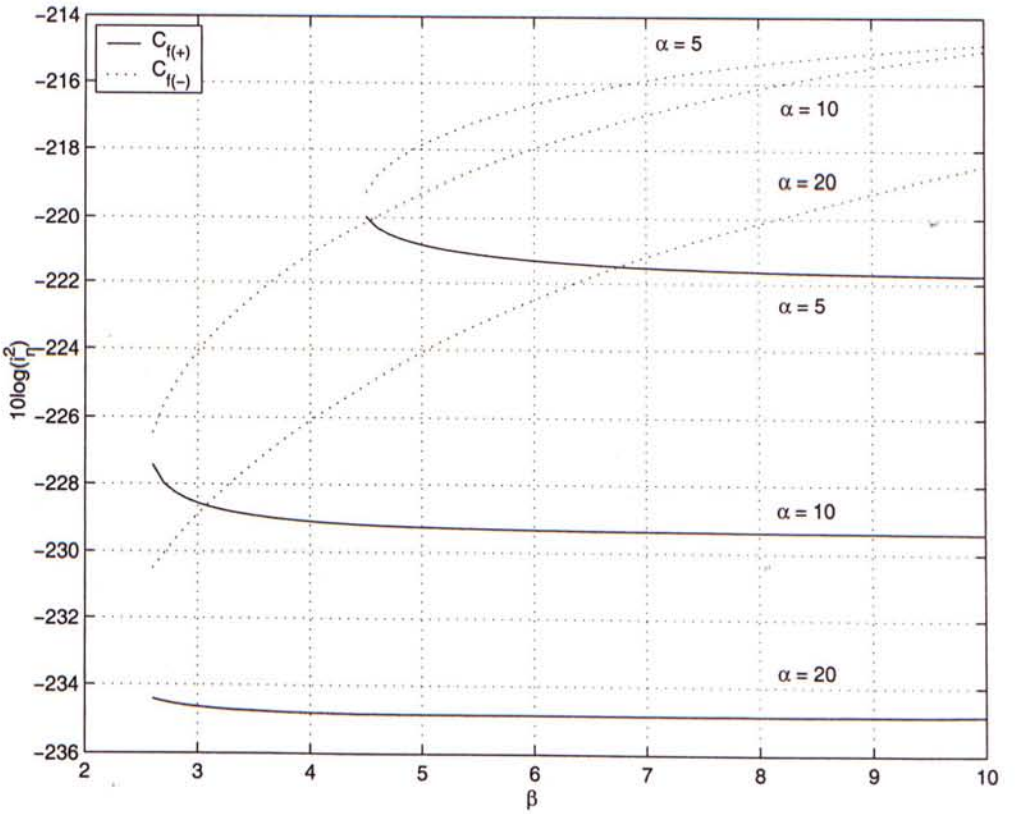

Fig. 6.2 Noise Current as a function of α and β

6.2 Noise Figure of the Passive Filter

Fig. 6.3 shows the noise equivalent circuit of the second-order coupled-resonator filter. The noise current i_{nr1} and i_{nr2} generated by the resonator are given by (5.5).

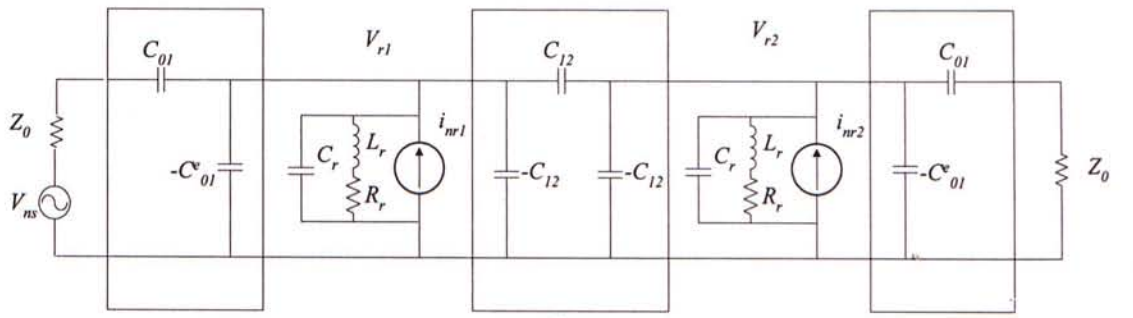

Fig. 6.3 Noise model of passive filter

The corresponding noise current flowing through the load are therefore described by,

$$i_{nr1o} = \frac{i_{nr1} j\omega C_{12}}{(\omega C_{12})^2 + (\omega C_{12} + Y_r)^2} \frac{j\omega C_{01}}{(1 + j\omega C_{01} Z_0)} \tag{6.4}$$

$$i_{nr2o} = \frac{i_{nr2} (\omega C_{12} + Y_r)}{(\omega C_{12})^2 + (\omega C_{12} + Y_r)^2} \frac{j\omega C_{01}}{(1 + j\omega C_{01} Z_0)} \tag{6.5}$$

where

$$Y_r = \frac{1}{j\omega L_r + R_r} + j\omega C_r$$

Note that i_{nr1}^2 is uncorrelated to i_{nr2}^2. Furthermore, the noise power generated by the loss resistance associated with the resonator is equal to,

$$\begin{aligned} P_{nr}(\omega) &= \left| i_{nr10} + i_{n2o} \right|^2 Z_0 \\ &= \left| \frac{j\omega C_{01}}{(1 + j\omega C_{01} Z_0)} \frac{1}{(\omega C_{12})^2 + (\omega C_{12} + Y_r)^2} \right| \\ &\quad \left| i_{nr1} j\omega C_{12} + i_{nr2} (\omega C_{12} + Y_r) \right|^2 Z_0 \\ &= \frac{\omega C_{12}}{\left| (\omega C_{12})^2 + (\omega C_{12} + Y_r)^2 \right|^2} \left[\left| \omega C_{12} \right|^2 + \left| \omega C_{12} + Yr \right|^2 \right] \overline{i_{nr}^2} \end{aligned} \tag{6.6}$$

where

$$\overline{i_{nr1}^2} \approx \overline{i_{nr2}^2} = \overline{i_{nr}^2}$$

It can be further shown that the power gain G_A of the passive filter is given as

$$G_A(\omega) = \frac{4(\omega C_{12})^4}{\left|(\omega C_{12})^2 + (\omega C_{12} + Y_r)^2\right|^2} \tag{6.7}$$

Thus, the noise figure of the passive filter is

$$\begin{aligned} NF_{pass}(\omega) &= 1 + \frac{P_{nr}}{G_A kT} \\ &= 1 + \frac{|\omega C_{12}|^2 + |\omega C_{12} + Y_r|^2}{4kT(\omega C_{12})^3} \end{aligned} \tag{6.8}$$

If we set $\omega = \omega_0$, and assuming that $Y_r \approx g_o$, we obtain

$$\begin{aligned} NF_{pass}\big|_{\omega=\omega_0} &= 1 + \frac{\left[(\omega_0 C_{12})^2 + (\omega_0 C_{12} + g_o)^2\right]\overline{i_{nr}^2}}{4kT(\omega_0 C_{12})^3} \\ &= 1 + \frac{\left[(\omega_0 C_{12})^2 + (\omega_0 C_{12} + g_o)^2\right]g_o}{(\omega_0 C_{12})^3} \end{aligned} \tag{6.9}$$

$$G_A\big|_{\omega=\omega_0} = \frac{4(\omega_0 C_{12})^4}{\left|(\omega_0 C_{12})^2 + (\omega_0 C_{12} + g_o)^2\right|^2} \tag{6.10}$$

Fig. 6.4 shows the plot of Noise Figure and insertion loss ($-G_A$) of the passive filter, assuming $R_r = 0.6\Omega$, $Q = 20$ at 900MHz. From the diagram, it can be observed that the noise figure (9.18 dB) is almost the same as the insertion loss value (9.47dB) of the filter at the center frequency. However, this relationship no longer holds when $\omega \neq \omega_0$.

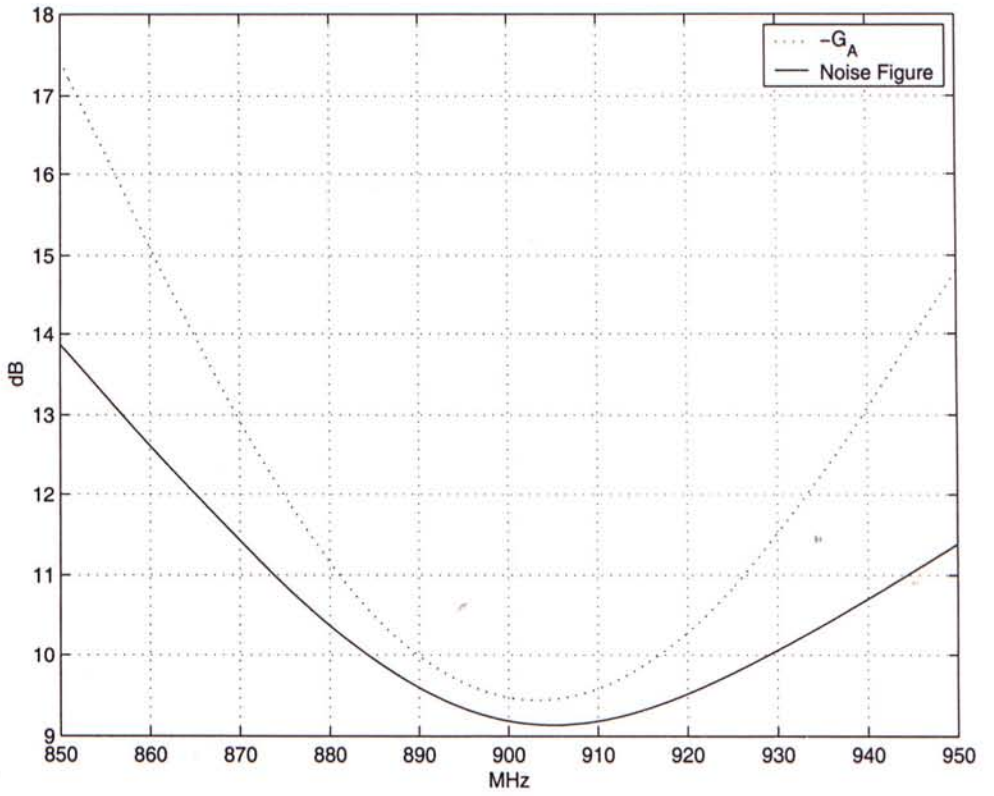

Fig. 6.4 Loss and noise figure of the passive filter

6.3 Noise Figure of the Active Filter

In this section, the noise figure of a second-order, third-order and forth-order active filter is derived. A method to optimize the noise figure is also introduced.

6.3.1 Noise Figure of a Second-order Active Filter

Fig. 6.5 shows the circuit of the second-order active filter with the presence of all noise source including noise current produced by the active devices as well as the loss resistance of the resonator (i_{nk} and i_{nrk}, $k = 1,2$) within the filter is also shown.

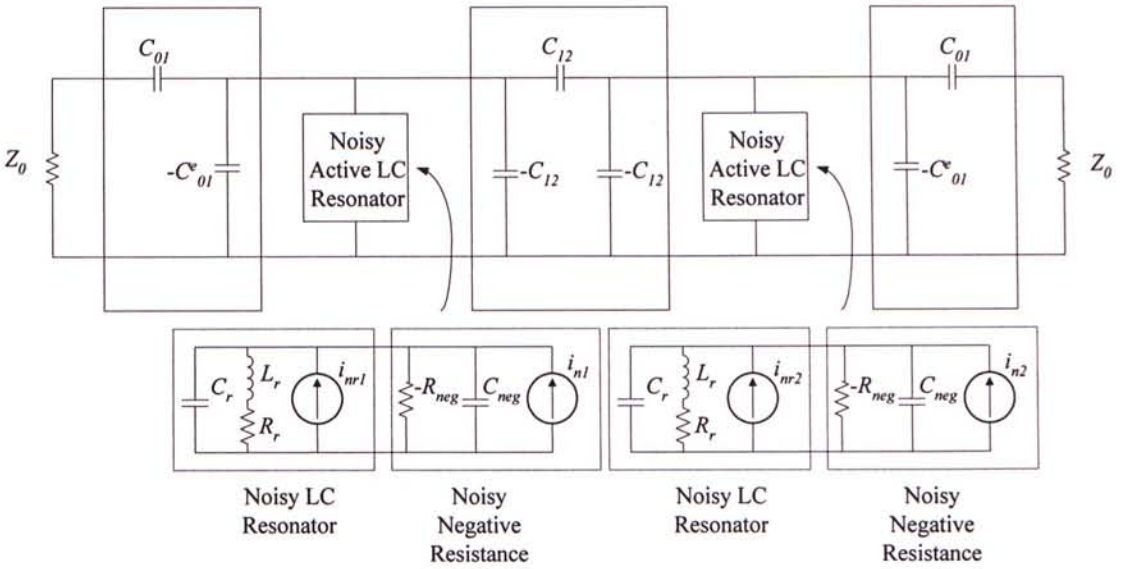

Fig. 6.5. Noise model of second order active filter

Note that all the noise current sources are uncorrelated and in *rms* value.

According to (4.10), the noise power delivered to the load can be written as,

$$\begin{aligned} P_{noise}\big|_{N=2} &= \frac{\left|ji_{noise1} + i_{noise2}\right|^2}{4\omega_0 C_{12}} \\ &= \frac{\overline{i^2_{noise}}}{2\omega_0 C_{12}} \\ &= \frac{\sqrt{2}}{2}\omega_0 L_r \frac{\omega_0}{BW}\overline{i^2_{noise}} \end{aligned} \tag{6.11}$$

where

$$\overline{i^2_{noise}} = \overline{i^2_{nrk}} + \overline{i^2_{nk}} \qquad (k = 1, 2)$$

Thus the noise figure of the active filter is

$$\begin{aligned} NF_{active}\big|_{N=2} &= 1 + \frac{P_n}{kT} = \\ &= 1 + \frac{\sqrt{2}}{2kT}\omega_0 L_r \frac{\omega_0}{BW}\overline{i^2_{noise}} \end{aligned} \tag{6.12}$$

Combining expression (6.12) with (5.29) - (5.31) and (6.1), we get

$$NF_{active}\big|_{N=2} = 1+\sqrt{2}\omega_0 L_r \frac{\omega_0}{BW}\times \left\{ 2g_o + \frac{\frac{2(\omega_0 C_{gs})^2 R}{g_m}\left[\frac{C_f}{C_T}(\alpha-2)-1\right]+2g_m P-\frac{cor}{kT}\frac{\alpha}{\beta}}{\alpha\frac{C_f}{C_T}} \right\} \tag{6.13}$$

Furthermore, the noise behavior of the filter at any frequency $\omega(\omega \neq \omega_0)$ within the operating bandwidth of the filter, is given by

$$\begin{aligned} P_{noise}(\omega)\big|_{N=2} &= \frac{\omega C_{12}}{\left|(\omega C_{12})^2+(\omega C_{12}+jB_r)^2\right|^2}\left[\left|\omega C_{12}\right|^2+\left|\omega C_{12}+jB_r\right|^2\right]\overline{i_{nr}^2} \\ &= \frac{\omega C_{12}}{\left|(\omega C_{12})^2+(\omega C_{12}+jB_r)^2\right|^2}\left[2\left|\omega C_{12}\right|^2+\left|B_r\right|^2\right]\overline{i_{nr}^2} \end{aligned} \tag{6.14}$$

where

$$\begin{aligned} jB_r &= \frac{1}{j\omega L_r}+j\omega C_r \\ &= j\omega C_r\left(\frac{\omega^2-\omega_0^2}{\omega^2}\right) \\ NF_{active}(\omega)\big|_{N=2} &= 1+\frac{P_{nr}(\omega)}{G_A(\omega)kT} \\ &= 1+\frac{\overline{i_{noise}^2}}{2kT\omega C_{12}}+\frac{B_r^2\overline{i_{noise}^2}}{4kT(\omega C_{12})^3} \\ &= 1+\frac{\overline{i_{noise}^2}}{\sqrt{2}kT\omega}\frac{\omega_0}{BW}\omega_0^2 L_r \\ &\quad +\frac{\overline{i_{noise}^2}}{\sqrt{2}kT\omega}\left(\frac{\omega_0}{BW}\right)^3\omega_0^2 L_r\left(\frac{\omega^2-\omega_0^2}{\omega^2}\right)^2 \end{aligned} \tag{6.15}$$

From the above expression, we can see that when $\omega \neq \omega_0$, the noise figure of the filter increases with the square of frequency offset. Moreover, the bandwidth of

the filter has a strong effect on noise figure. Fig. 6.6 shows the variations of the computed noise figure versus frequency $\alpha = 10$, $\beta = 5$ and the extracted values of P, R, C in table 5.4. The figure shows that a large feedback capacitance value should be chosen, $C_{f(+)}$ for low noise figure of the active filter.

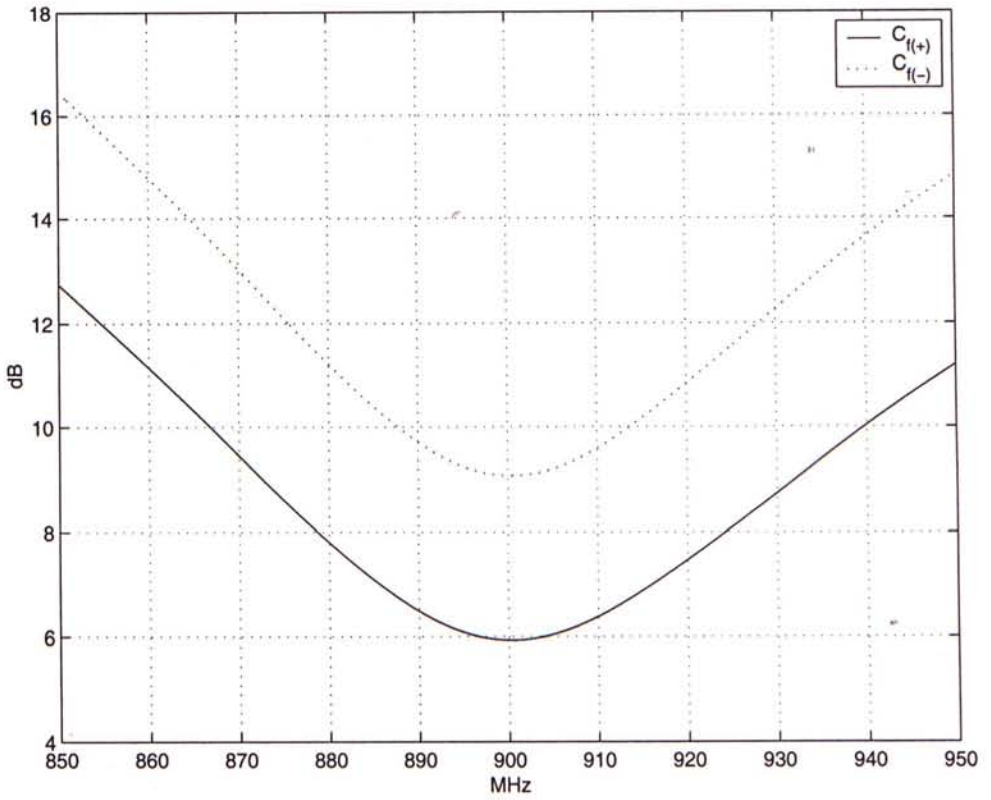

Fig. 6.6. Noise figure of the active filter combing with (3.11), $\alpha = 10$, $\beta = 5$

6.3.2 Noise Figure of higher-order Active Filter

The noise figure of the third- and forth-order active filter is similar to that of second order active filter. Assume all the noise power produced by individual active LC-resonator are similar and denote them by $\overline{i_{noise}^2}$. Hence, the noise power delivered

to the load, for third-order active filter, is given by

$$P_{noise}\Big|_{N=3} = \frac{\sqrt{2}}{4\omega_0 C_{12}}\left|\frac{-i_{noise1}+i_{noise3}}{\sqrt{2}} + ji_{noise2}\right|^2$$
$$= \frac{\sqrt{2}}{2\omega_0 C_{12}}\overline{i_{noise}^2} \qquad (6.16)$$
$$= \omega_0 L_r \frac{\omega_0}{BW}\overline{i_{noise}^2}$$

The noise figure of the third-order active filter is thus

$$NF_{active}\Big|_{N=3} = 1+\omega_0 L_r \frac{\omega_0}{BW}\times \left\{\frac{\frac{4(\omega_0 C_{gs})^2 R}{gm}\left[\frac{C_f}{C_T}(\alpha-2)-1\right]+4g_m P-\frac{2Cor}{kT}\frac{\alpha}{\beta}}{\alpha\frac{C_f}{C_T}}+4g_o\right\} \qquad (6.17)$$

For the forth-order active filter, the noise power delivered to the load from the resonator is

$$P_{noise}\Big|_{N=4} = \frac{\omega_0 C_{12}^2}{4\omega_0 C_{23}}\left|\frac{-ji_{noise1}+i_{noise4}}{\omega_0\frac{C_{12}^2}{C_{23}}}+\frac{-i_{noise2}+ji_{noise3}}{\omega_0 C_{12}}\right|^2$$
$$= \frac{\omega_0 C_{12}^2}{4\omega_0 C_{23}}\left[\frac{1}{\left(\omega_0\frac{C_{12}^2}{C_{23}}\right)^2}+\frac{1}{(\omega_0 C_{12})^2}\right]\overline{i_{noise}^2} \qquad (6.18)$$
$$= \frac{1}{2}\omega_0 L_r \frac{\omega_0}{BW}(0.7654+1.848)\overline{i_{noise}^2}$$

The noise figure of the forth-order active filter is thus

$$NF_{active}\big|_{N=4} = 1+(0.7654+1.848)\omega_0 L_r \frac{\omega_0}{BW}\times \left\{\frac{\frac{2(\omega_0 C_{gs})^2 R}{gm}\left[\frac{C_f}{C_T}(\alpha-2)-1\right]+2g_m P-\frac{Cor}{kT}\frac{\alpha}{\beta}}{\alpha\frac{C_f}{C_T}}+2g_o\right\} \quad (6.19)$$

By observing (6.11), (6.16) and (6.18), we can see that the noise power delivered to the load of the N^{th} ($N = 2, 3$ and 4)-order active filter can be expressed as,

$$P_{noise}\big|_N = \frac{(g_1+g_2+\ldots g_N)}{4}\omega_0 L_r \frac{\omega_0}{BW}\overline{i^2_{noise}} \quad (6.20)$$

The noise figure of the active filter can then be re-expressed as,

$$NF_{active}\big|_N = 1+(g_1+g_2+\ldots g_N)\omega_0 L_r \frac{\omega_0}{BW}\times \left\{g_o+\frac{\frac{(\omega_0 C_{gs})^2 R}{g_m}\left[\frac{C_f}{C_T}(\alpha-2)-1\right]+g_m P-\frac{cor}{2kT}\frac{\alpha}{\beta}}{\alpha\frac{C_f}{C_T}}\right\} \quad (6.21)$$

The above expression reveals the influence of device parameters, component values, and filter characteristics on noise figure of the filter circuit as follows.

1. Fig. 6.7 shows the plot of NF_{active} (dB) as a function of α and β. It can be seen from the diagram that $C_{f(+)}$ should be chosen for low noise performance.

2. Large value of α is also required for low noise figure of the filter but there is no significant reduction when α is greater that 10.

3. Losses within the passive part of the filter, characterized by the inductor Q-factor,

have direct effect on the noise figure of the filter. Equation (6.21) indicates that the noise figure decreases with increasing Q-factor (decreasing g_o)

4. The noise figure of the filter is inversely proportional to the bandwidth of the filter.

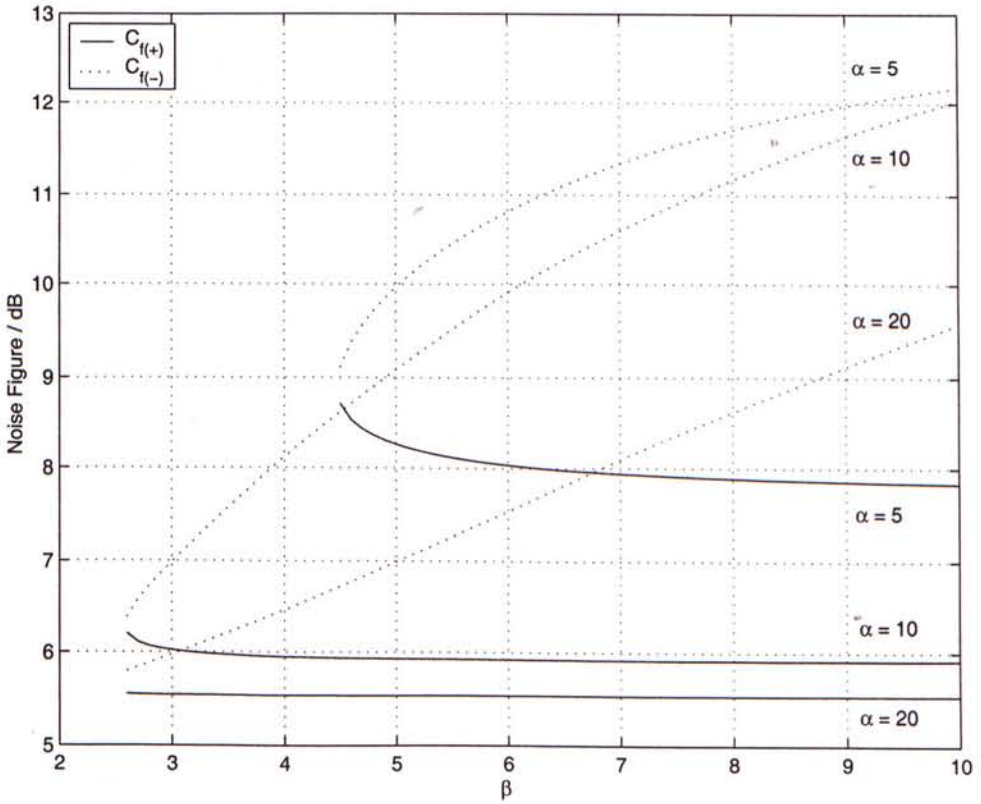

Fig. 6.7 Noise figure of the active filter as a function of α and β

6.4 Active Filter Design with Simultaneous Noise and Linearity Performance Consideration

The analysis of nonlinear and noise behavior of the active filter has been performed in chapter 4 and previous sections. Design considerations on the design of

the active may be concluded as follows,

1. The bandwidth of the filter has strong effect on both IM and noise performance. They are both inversely proportional, with different order, to the bandwidth.
2. Both IMD and noise performance can be improved by employing high Q inductors.
3. According to Fig. (4.6) and Fig. (6.6), $C_{f(+)}$ should be chosen for low noise figure value. In addition, larger value of α can reduce both the noise figure and IMD of the filter. β has little effect on both noise and IM performance.
4. $C_{f(-)}$ should be used for low IMD. Large value of α can further decrease the IMD.

Chapter 7 Design of 900MHz Hybrid Active Filter

In previous chapters, the design equations of the coupled resonator band-pass filter are derived with respect to the choice of transconductance g_m, the external gate-to-source capacitance C_{ext}, and the feedback capacitance C_f in the negative resistance circuit. It has also been shown that the reduction of noise figure of the active filter can be achieved by proper choice of feedback capacitance.

Two experimental hybrid active filters are constructed and their basic filter properties, nonlinear characteristics and noise figure are measured. The designs of these filters are based upon different choice of C_f values. The aim of this experiment is to validate the noise analysis that has been carried out in chapter 6.

7.1 Schematic of the Active Filter

Fig. 7.1 shows the schematic of the second order active filter. Note that a RF choke (L_{path}) is connected in parallel with the feedback capacitor to provide a DC path to ground for the MESFET. The effective value of the feedback capacitance is

$$C_f = C_{f0} - \frac{1}{\omega^2 L_{path}} \tag{7.1}$$

where

C_{f0} = actual feedback capacitance used

C_f = equivalent feedback capacitance

The PCB layout of the above circuit is depicted in Fig. 7.2. Factors such as ground planes, via holes, line width, trace routing and component spacing affect the performance of the constructed filter.

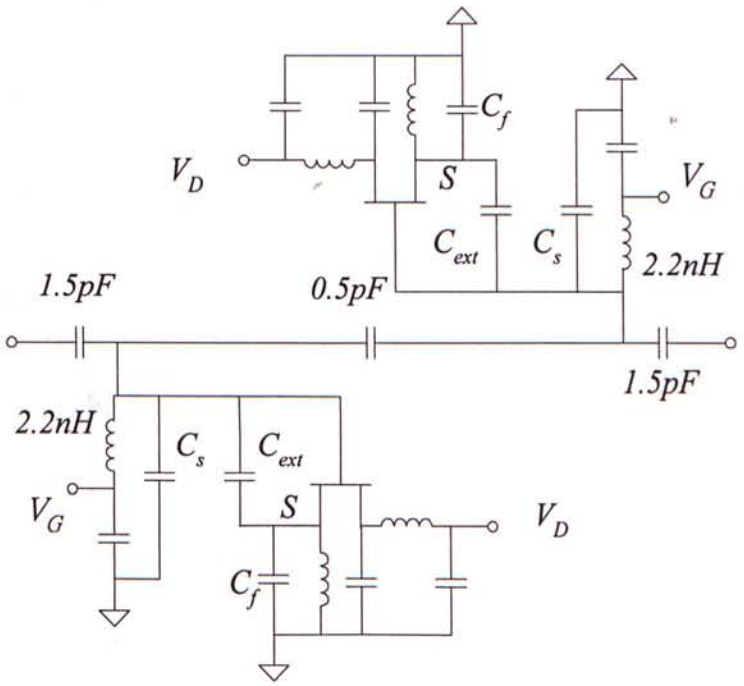

Fig. 7.1 Schematic of the second order active filter

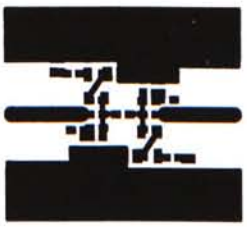

Fig. 7.2 PCB layout of the second order active filter

7.2 Procedures of Circuit Assembly

Assembly procedures of the active filter are summarized as follows:

1. Construction of the passive filter
2. Addition of the negative resistance circuit
3. Selection of external gate-to-source capacitance, C_{ext}
4. Tuning of C_f until zero insertion loss is achieved within the filter's pass-band
5. Adjustment of Cs in the resonator to the fine-tune the center frequency

The two last steps are repeated until zero insertion loss is obtained while the center frequency is kept around 900MHz.

7.3 Measurement Results

The measured performances of the passive filter and active filter are presented in this session. For the active filter measurement, all the MESFETs are biased with drain voltage equal to 3V and drain current of 10mA. This setting ensures the operating condition of all the MESFETs are similar to each other.

7.3.1 Passive Filter

Fig. 7.3 shows the physical construction of the lumped-element passive filter circuit using surface-mount devices. The frequency response of the passive filter was measured before the addition of the negative circuit. The *S*-parameter and noise figure

characteristic of the passive filter circuit are measured using HP8510C network analyzer and HP9070B noise figure meter, respectively.

Fig. 7.4 shows the measurement result of the passive filter. It is found to have a noise figure of 7.1dB and an insertion loss of about 8.8dB at the center of the pass-band. The input and output return loss are both better than 10 dB over most of the pass-band range.

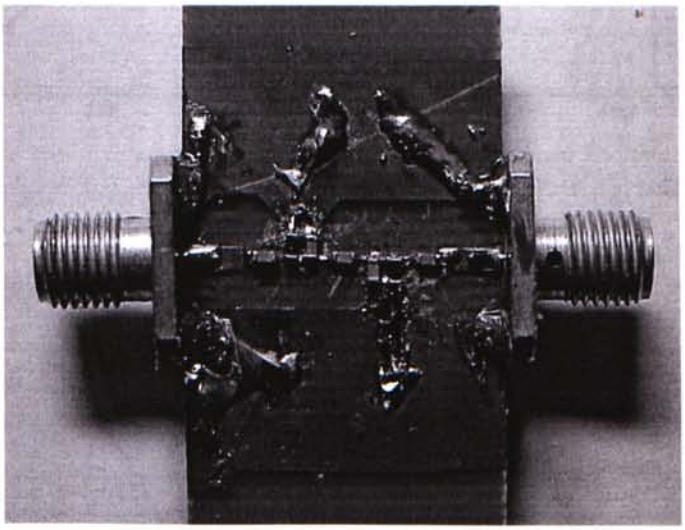

Fig. 7.3 Experimental passive filter circuit

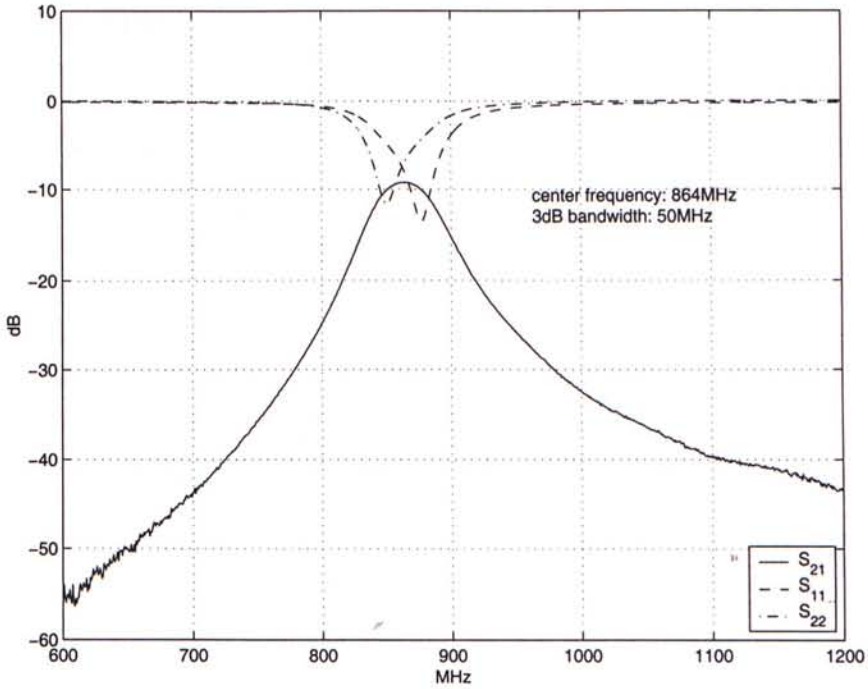

Fig. 7.4 *S*-parameters of the passive filter

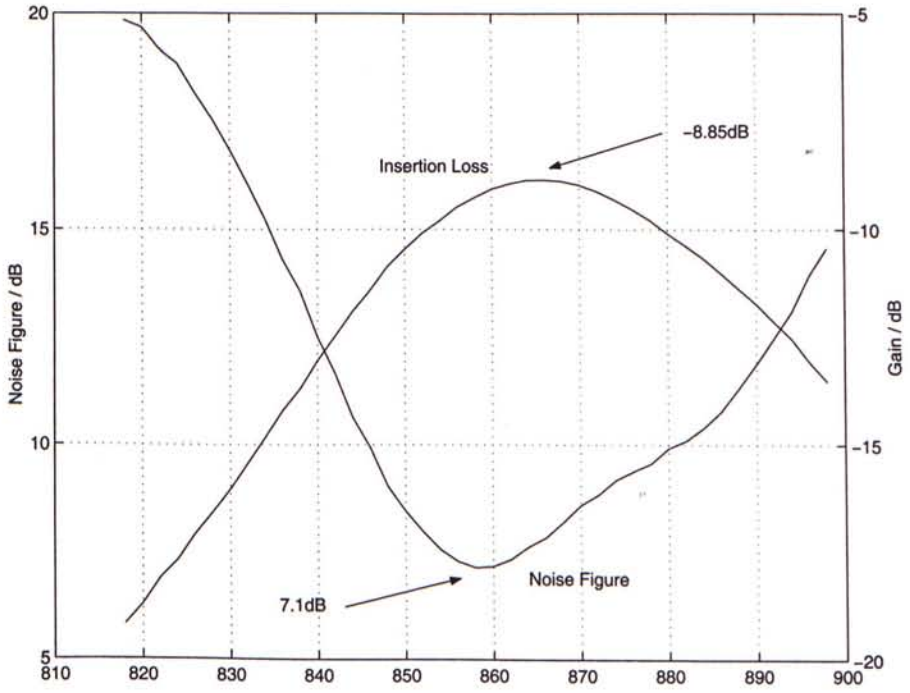

Fig. 7.5 Noise figure and gain of the passive filter

7.3.2 Active Filter

With the addition of negative resistance circuits to the passive filter, two active filters with different C_f are constructed. The circuit parameters of the filter are tabulated in table 7.1 and the physical appearance of the filter circuit is given in Fig. 7.6.

For comparison, the frequency response, IM performance and the noise behavior of the two active filters are all measured and plotted in Fig, 7.5 to. 7.8. Fig. 7.5 shows that the filters exhibit zero insertion loss at the center of the pass-band and excellent input and output return loss within the 3 dB bandwidth. The center frequencies and bandwidths of the two circuits are slightly different due to availability and tolerances of the components.

In addition, it can be observed from Fig. 7.7 that the 3rd IMD power of the active filter can be reduced by nearly 20dB at low input power level (<-16dBm), by selecting $C_{f(-)}$ as the feedback capacitance.

Finally, Fig. 7.8 and 7.9 indicate that the noise figure of the active filter is reduced from of 9dB to 5.5dB when the larger feedback capacitance value (8.9pF) is chosen.

	C_{f0} / pF	L_{path} / nH	C_f / pF(7.1)	C_s / pF	C_{ext} / pF	f_0 / MHz
Circuit 1	12	10	8.9	7	2	900
Circuit 2	4	10	0.87	8	2	940

Table 7.1 Circuit parameters of the two active filters

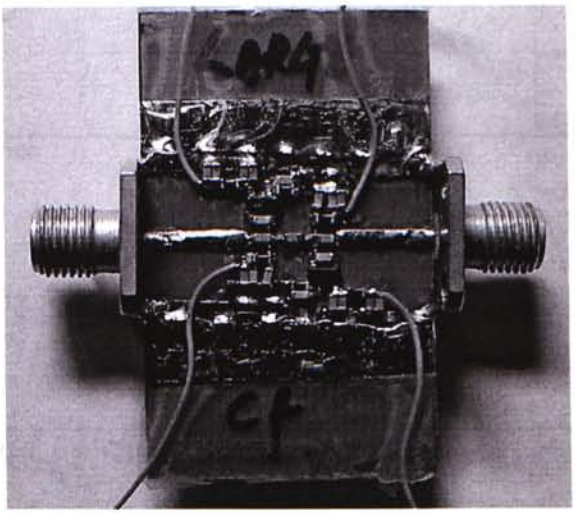

Fig. 7.6 Experimental active filter circuit

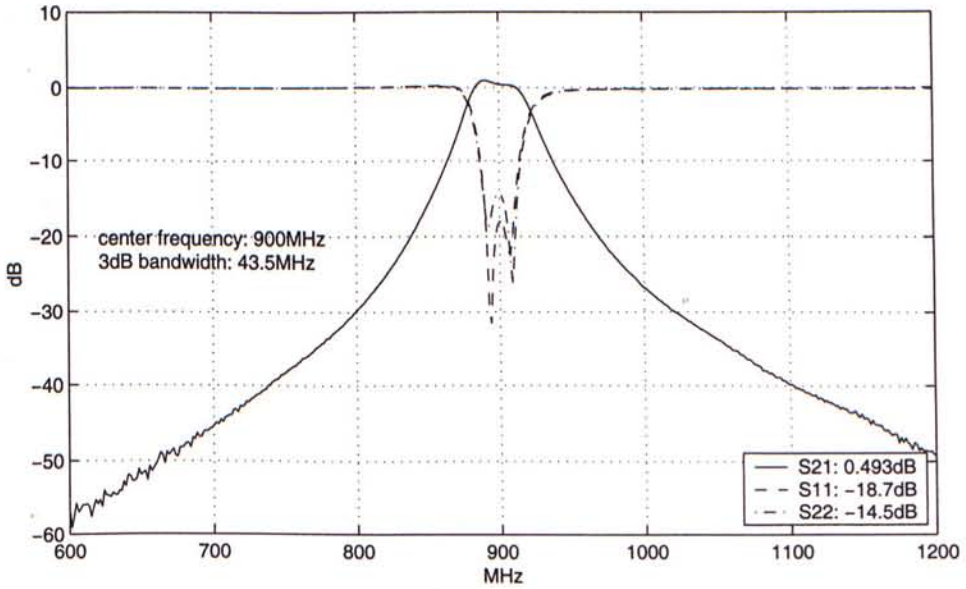

Fig. 7.7 *S*-parameters of circuit 1 (C_f = 8.9pF)

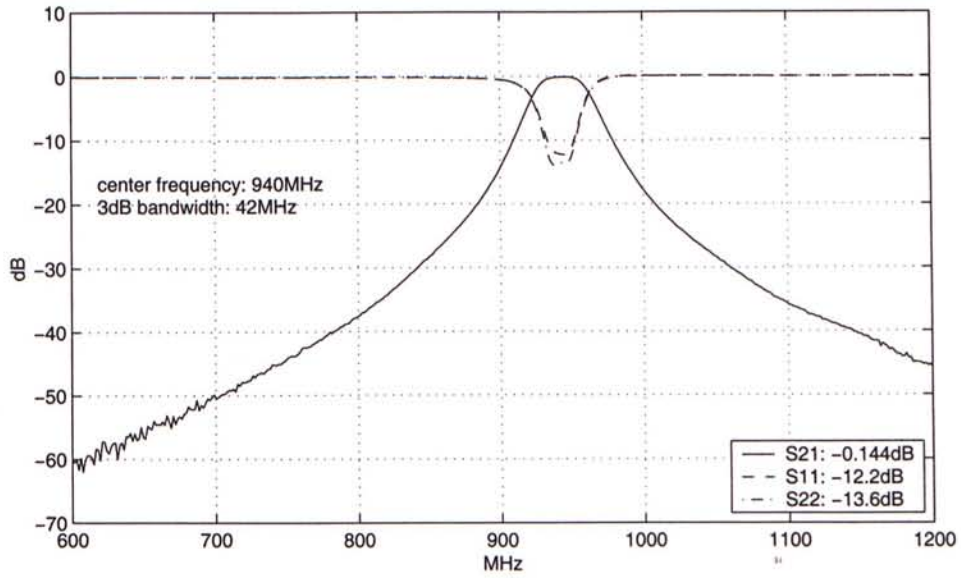

Fig. 7.8 *S*-parameters of circuit 2 (C_f = 0.87pF)

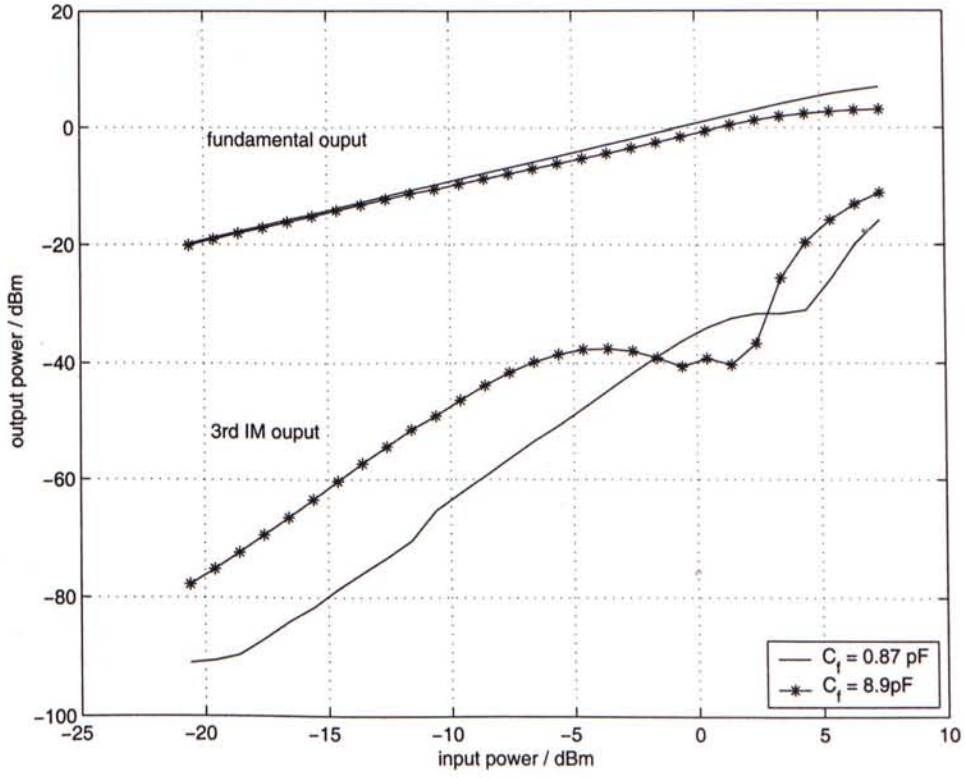

Fig. 7.9 Comparison of measured IMD levels of circuit 1 and circuit 2

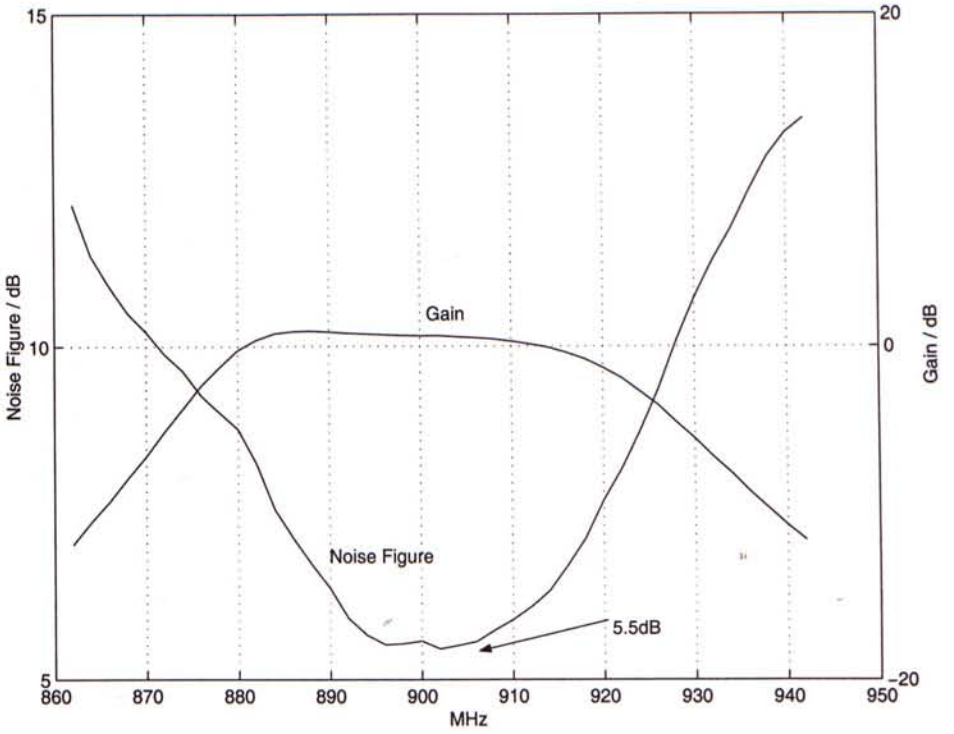

Fig. 7.10 Noise figure of circuit 1 (C_f = 8.9pF)

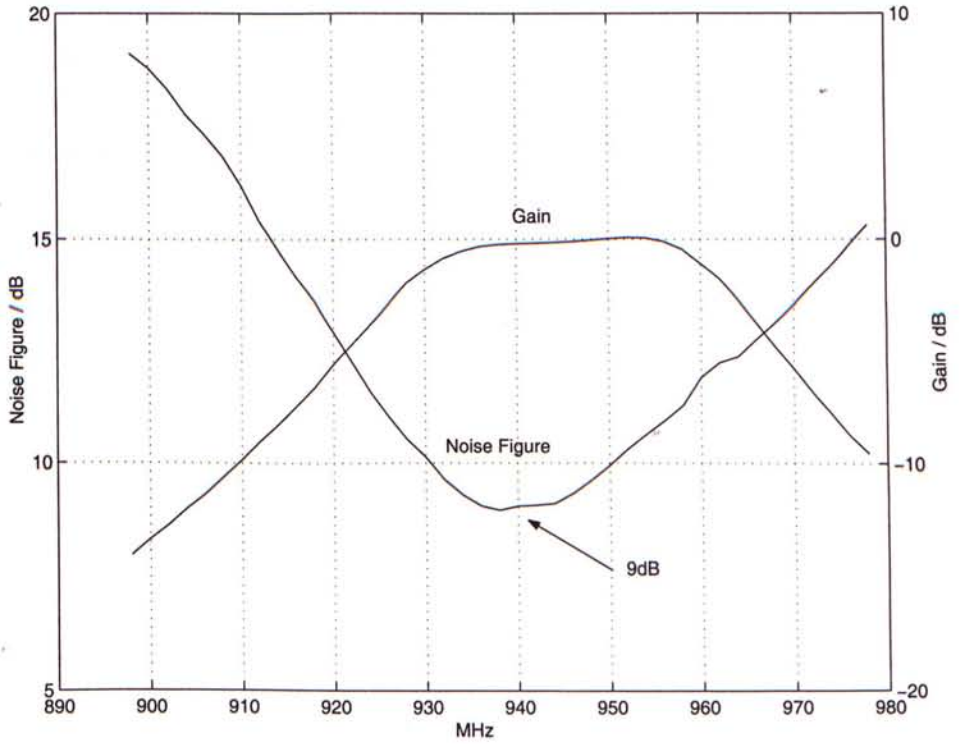

Fig. 7.9 Noise figure of circuit 2 (C_f = 0.87pF)

For a better comparison of the two circuits, the power levels of the 3rd IMD of the active filters at input power = -15dBm and –5dBm, the extrapolated IP_3 and noise figure of the active filter are tabulated in table 7.2

	C_f / pF	I/P = -15dBm 3rd IM / dBm	I/P = -5dBm 3rd IM / dBm	IP_3 (input) / dBm	NF_{min} / dB
Circuit 1	8.9	-62	-38	8	5.5
Circuit 2	0.87	-82	-52	16	9

Table 7.2 Comparison of the two active filters on IM and noise performance

From the above result, we can see that there is trade off between the noise and linearity performance of the active filter. For circuit 1, large C_f results in low noise figure but poor linearity. On the other hand, circuit 2 with small C_f results in better linearity but higher noise figure. Thus, either noise or linearity performance has to be sacrificed for optimal active filter design.

Chapter 8 Conclusion and Future Work

The main contributions of this research can be concluded as follows.

1. The basic requirement on the selection of circuit parameters (g_m, C_{gs} and C_f) are derived for zero insertion loss of the filter.
2. The noise behavior of the active filter has been addressed. An expression for predicting the noise figure of the active filter is derived.
3. A method to reduce the noise figure of active filters is proposed and verified experimentally.
4. Finally, optimized active filter design by considering the linearity and noise performance of the active filter is discussed.

For future work, a practical implementation of these filters based upon MMIC technology is necessary. Furthermore, the noise and IMD performances of other classes of active filter may also be analyzed in a similar fashion to identify the best filter topology for a particular application.

References

[1] G. L. Matthaei, L. Young, and E. M. T. Jones, *Microwave Filter Impedance Matching Networks and Coupling Structures*, New York: McGraw-Hill, 1964.

[2] Eric C. Krantz and G. R. Branner, "Active microwave filters with noise performance considerations," *IEEE Trans. Microwave Theory Tech.*, vol. 42, pp. 1368-1379, July 1994.

[3] S.E. Sussman-Fort, "A realization of a GaAs Microwave active filter," *IEEE Trans. Microwave Theory Tech.*, vol. 37, pp. 1418-1424, Sept. 1989.

[4] R. R. Bonetti and A. E. Williams, "An octave-band MMIC active filter," *IEEE MTT-S int. Microwave Symp. Dig.*, vol. 2, pp. 823-826, May 1990.

[5] C.Y. Chang and Tatsuo Itoh, "Microwave active filters based on coupled negative resistance method," *IEEE Trans. Microwave Theory Tech.*, vol. 38, pp. 1879-1884, Dec. 1990.

[6] B. p. Hopf, i. Wolff and M. Guglielmi, " Coplanar MMIC active bandpass filters using negative resistance circuits," *IEEE Trans. Microwave Theory Tech.*, vol. 42, pp. 2598-2602 Dec. 1994.

[7] U. Karacaoglu and I. D. Robertson, "MMIC active bandpass filters using varactor-tuned negative elements," *IEEE Trans. Microwave Theory Tech.*, vol. 43,

pp. 2926-2932, Dec. 1995.

[8] Y. H. Cho, S. C. Hong and Y. S. Kwon, "A low-power monolithic GaAs FET bandpass filter based on negative resistance technique," *IEEE Microwave Guided Wave Lett.*, vol. 8, pp. 161-163, Apr. 1998.

[9] K. K. M. Cheng and S. C. Chan, "Reduction of intermodulation distortion in microwave active bandpass filters, theory and experiments," *IEEE Trans. Micowave Theory Tech.*, vol. 48, pp. 221-225, Feb. 2000.

[10] M. R. Moazzam and A. H. Agvami, "Analysis and design of a novel microwave active filter," *IEEE Antennas Propagat Soc. Symp. Dig.*, vol. 1, June 1991.

[11] W. Schwab and W. Menzel, "A low-noise active bandpass filter," *IEEE Microwave Guided Wave Lett.*, vol. 3, pp. 1-2, Jan. 1993.

[12] C. Rauscher, "Microwave active filters based in transversal and recursive principles," *IEEE Trans. Microwave Theory Tech.*, vol. 33, pp. 1350-1360, Dec. 1985.

[13] M. J. Schindler and Y. Tajima, "A novel MMIC active filter with lumped and transversal elements," *IEEE Trans. Microwave Theory Tech.*, vol. 37, pp. 2148-2153, Dec. 1989.

[14] M. Danestig, H. Johansson, A. Ouacha and S. Rudner, "Low-noise active recursive MMIC filters," *IEEE MTT-S Int. Microwave Symp. Dig.*, Vol. 2, pp.

705 –708, June, 1997.

[15] H. Ezzedine, L. Billonnet, B. Jarry, and P. Guillon, "Optimization of noise performance for various topologies of planar microwave active filters using noise wave techniques," *Microwaves Trans. Theory Tech.*, vol. 46, Dec. 1998.

[16] S. Hara, T. Tokumitsu, T. Tanaka, and M. Aikawa, "Broadband monolithic microwave active inductor and application to a miniaturized wideband amplifier," *IEEE MTT-S Int. Microwave Symp. Dig.*, vol. 1, May 1988, pp. 107-110.

[17] S. Hara, T. Tokumitsu and M. Aikawa, "Losses, broadband monolithic microwave active inductors, " *IEEE MTT-S Int. Microwave Symp. Dig.*, vol. 3, pp. 955-958.

[18] Y. Ishikawa, S. Yamashita and S. Hidaka, "Noise design of active feedback resonator BEF," IEEE Trans. *Microwave Trans. Theory Tech.*, vol. 41, pp.2133-2138, Dec. 1993.

[19] Stephen A. Maas, "Nonlinear Microwave Circuits," Artech House, 1988

[20] H. Rothe, and W. Dahlke, "Theory of noisey fourpoles," *Proc. IRE.*, vol. 44, pp. 811-818, June 1956.

[21] H. Hillbrand and P. H. Russer, "An efficient method for computer aided noise analysis of linear amplifier networks," *IEEE Trans. Circuits Syst.*, vol. CAS-23,

pp. 235-238, Apr. 1976.

[22] A. Van Der Ziel, "Thermal noise in field-effect transistor," *Proc. IRE.*, vol. 50, pp. 1808-1812, 1962.

[23] A. Van Der Ziel, "Gate noise in field effect transistors at moderately high frequencies," *Proc. IRE.*, vol. 51, pp. 461-467, 1963.

[24] H. Statz, H. A. Haus, and R. A. Pucel, "Noise characteristic of gallium arsenide field-effect transistors," *IEEE Trans. Electron Devices*, vol. 21, Sept. 1974.

[25] A. Riddle, "Extraction of FET model noise-parameters from measurement," *IEEE MIT-S Int. Microwave Symp. Dig.*, vol. 2, pp. 1113-1116, June 1991

[26] C. W. Fan, "Unified Volterra Series Analysis of Injection Locked Oscillators," M.Phil. thesis, CUHK, 1998.

Author's Publication

[1] K. K. M. Cheng, H. Y. Chan, and K. Y. Yip, "Optimization of linearity and noise performances of microwave active filters," to appear, 2000 Asia-Pacific Microwave Conference.

[2] K. K. M. Cheng, and H. Y. Chan, "Noise performance of negative resistance compensated microwave band-pass filters: Theory and experiments," to appear, IEEE Trans. Microwave Theory and Techniques.